JOURNAL OF STRUCTURAL BIOLOGY **121,** 142–161 (1998)
ARTICLE NO. SB983945

Electron Crystallography of Two-Dimensional Crystals of Membrane Proteins

Thomas Walz[1]

Krebs Institute for Biomolecular Research, Department of Molecular Biology and Biotechnology, University of Sheffield, Firth Court, Western Bank, Sheffield, S10 2TN, United Kingdom

and

Nikolaus Grigorieff

Laboratory of Molecular Biology, Medical Research Council, Hills Road, Cambridge, CB2 2QH, United Kingdom

Received December 10, 1997

Electron microscopy has become a powerful technique, along with X-ray crystallography and nuclear magnetic resonance spectroscopy, to study the three-dimensional structure of biological molecules. It has evolved into a number of methods dealing with a wide range of biological samples, with electron crystallography of two-dimensional crystals being so far the only method allowing data collection at near-atomic resolution. In this paper, we review the methodology of electron crystallography and its application to membrane proteins, starting with the pioneering work on bacteriorhodopsin, which led to the first visualization of the secondary structure of a membrane protein in 1975. Since then, improvements in instrumentation, sample preparation, and data analysis have led to atomic models for bacteriorhodopsin and light-harvesting complex II from higher plants. The structures of many more membrane proteins have been studied by electron crystallography and in this review examples are included where a resolution of better than 10 Å has been achieved. Indeed, in some of the given examples an atomic model can be expected in the near future. Finally, a brief outlook is given on current and future developments of electron crystallographic methods.

INTRODUCTION

Electron microscopy is one of the most versatile and direct techniques used to obtain information about the three-dimensional (3-D) structure of a specimen in the solid state. It has been a standard technique in material science for several decades where it promoted the rapid development of new materials for the engineering and semiconductor industry. In biology, electron microscopy has been applied to a large variety of specimens ranging from small protein molecules to thin sections of whole cells. In contrast to most samples in material science, a typical biological specimen exhibits variability and flexibility in its shape, and it is composed mainly of light atoms like hydrogen, carbon, nitrogen, and oxygen. Due to the very high water content of biological specimens, special care is needed to prevent loss of fine structure by dehydration in the vacuum of the electron microscope. Moreover, irradiation by high-energy electrons breaks chemical bonds, leading to a rapid degradation of the sample into its chemical components. Nevertheless, microscopy techniques have been developed which allow the 3-D structure of biological samples to be determined, with specimens ranging from macromolecules with a molecular weight of only some 10 kDa to very large assemblies. Indeed, high voltage microscopes (e.g., Porter, 1986) and the development of automated electron tomography (Dierksen *et al*., 1992; Koster *et al*., 1992a; Dierksen *et al*., 1993; Fung *et al*., 1996) have made it even possible in near native thin sections to look at organelles such as the mitochondrion (Renken *et al*., 1997) and the Golgi apparatus (Ladinsky *et al*., 1994) and to study the ultrastructural organization of macromolecular assemblies in specialized tissues such as the insect flight muscle (Schmitz *et al*., 1996), to name only a few examples. The visualization of these large structures makes

[1]To whom correspondence and reprint requests should be addressed. Fax: +44 (0)114 272 86 97. E-mail: T.Walz@Sheffield.ac.uk.

1047-8477/98 $25.00

electron microscopy a very powerful method in cell biology.

Electron microscopy can also provide 3-D information of small biological molecules at atomic or near-atomic resolution to determine their 3-D structure. X-ray crystallography and nuclear magnetic resonance (NMR) spectroscopy are techniques routinely used for this purpose, but their application is restricted either to crystals with sufficiently large dimensions and good crystalline order or to molecules with a maximum weight of about 30 kDa, respectively. A comparison of electron microscopy with X-ray crystallography and NMR spectroscopy is given in Chiu (1993).

Because it is possible to record images, an electron microscope can be used to obtain structural information of noncrystalline specimens such as single particles and filamentous structures. The lower size limit of an object to be studied by electron microscopy has been estimated based on a random atom model to be about 50 kDa (Henderson, 1995). Providing the particles are large enough to be aligned, averaging of images commonly yield molecular structures at the 20 Å level. Exceptions are the structures of highly symmetrical virus capsids which were determined to resolutions below 10 Å (Böttcher *et al*., 1997; Conway *et al*., 1997; Trus *et al*., 1997). The resolution obtained so far by electron microscopy of single particles and filaments is not sufficient to be interpreted at an atomic level. Nevertheless, in the case of molecular assemblies, a low resolution structure can still provide an envelope. Atomic structures of the individual components of the assembly determined by X-ray crystallography or NMR spectroscopy can then be fitted into the envelope to determine their mutual binding sites. Examples illustrating this point are the numerous complexes actin forms with its binding proteins (Rayment *et al*., 1993; McGough *et al*., 1994; Schmid *et al*., 1994), and the complexes of viruses with antibodies or receptors (e.g., Chiu and Smith, 1994; Rossman *et al*., 1994; Baker and Johnson, 1996; Smith *et al*., 1996).

Despite many years of development of a number of electron microscopical techniques for different types of biological specimens (for example tubular crystals such as those formed by the acetylcholine receptor which is reviewed in this issue by Nigel Unwin), so far only electron crystallography of two-dimensional (2-D) crystals has progressed to near-atomic resolution. Many proteins have been crystallized in 2-D (Jap *et al*., 1992; Kühlbrandt, 1992) and in some cases a structure could be obtained at atomic or near-atomic resolution using electron crystalloraphy. These include two membrane proteins (see below), and tubulin, a soluble protein (Nogales *et al*., 1998). Membrane proteins are usually too big to be studied by NMR, and they rarely form high quality 3-D crystals which can be used in X-ray crystallographic studies. However, since they form 2-D crystals in lipid bilayers much more readily, electron crystallography of 2-D crystals has acquired special importance in the structure determination of membrane proteins and this will be the subject of this review.

THE BEGINNING OF BIOLOGICAL ELECTRON CRYSTALLOGRAPHY

The development of electron crystallography of 2-D crystals is linked most intimately to the structure determination of bacteriorhodopsin (bR), the integral membrane protein forming the purple membranes in *Halobacterium salinarium* (formerly *Halobacterium halobium*). The 3-D structure determination of bR by electron crystallography, determined to 7 Å resolution in the membrane plane and to 14 Å resolution perpendicular to the plane (Henderson and Unwin, 1975; Unwin and Henderson, 1975), was the first direct visualization of the detailed structure of a transmembrane protein. This break-through came about by overcoming two major problems in electron crystallography. (i) The disruption and dehydration of the specimen in the vacuum of the electron microscope was strongly reduced by replacing water molecules with the less volatile glucose as an embedding medium. (ii) The effect of radiation damage due to the deposition of energy in the specimen by inelastically scattered electrons was minimized by using very low electron doses for the recording of images and electron diffraction patterns. Amplitudes were obtained by densitometry of electron diffraction patterns and computational analysis was used to extract phases from images. While the methods developed in 1975 were already good enough to record electron diffraction patterns out to a resolution of 3.5 Å, the phases from the images were obtained only to lower resolution. Thus, in the following years, efforts were made to determine the factors which degrade image quality and to reduce their effect (see below). Most of these factors have a more severe effect on images of tilted specimens which are needed for a 3-D reconstruction. Better recording techniques and improved image processing enabled Henderson and coworkers (1990) to determine the structure of bR at near-atomic resolution. This structure became the first model of a membrane protein solved by electron crystallography. The atomic model of light-harvesting complex II (LHC-II) from pea chloroplasts (Kühlbrandt *et al*., 1994) was the next structure of a membrane protein solved in this way, and together with several more membrane proteins currently underway (see below) electron crystallography of 2-D crystals has been

established as a general method. However, bR remains the ideal test specimen for further improvements of electron crystallography as illustrated, for example, by Bullough and Henderson (1990a), Grigorieff *et al.* (1996a), Kimura *et al.* (1997), and Mitsuoka *et al.* (submitted).

METHODOLOGY

It is not intended to give a full description of all the methods currently in use in electron crystallography because several accounts have already been written which describe the individual techniques in detail. This section outlines only the main techniques, thereby emphasizing the improvements made over the last few years.

Specimens Suitable for Electron Crystallography

Only very few proteins form 2-D crystals *in situ*, and the crystalline order and size of those occuring naturally are rarely good enough to be useful for structure determination at higher resolution. Even patches of the well-ordered purple membrane have to be artificially fused to form large areas ideal for electron diffraction experiments (Baldwin and Henderson, 1984). Therefore, the most widely used approach leading to specimens suitable for electron crystallography is to isolate and purify the protein of interest in a first step, and, in a second step, to induce formation of 2-D crystals which, ideally, are large, well-ordered, and single-layered. The current methods to produce 2-D crystals are extensively surveyed in Engel *et al.* (1992), Jap *et al.* (1992), and Kühlbrandt, (1992) and are also discussed in this issue by Hasler *et al.*

Specimen Preparation

Specimens for electron crystallography have to be prepared to prevent dehydration and disruption of the specimen in the vacuum of the electron microscope. In the first electron crystallographic studies of bR (Henderson and Unwin, 1975; Unwin and Henderson, 1975) glucose was used as an embedding medium, enabling diffraction spots to be observed out to 3.5 Å. Since then trehalose (Jap *et al.*, 1990a) and tannin (Wang and Kühlbrandt, 1991; Kühlbrandt *et al.*, 1994) have also been demonstrated to be suitable embedding media. Alternatively, Taylor and Glaeser (1974) showed that the fine structure of frozen-hydrated catalase crystals (ice embedded) is preserved to better than 3 Å resolution. Later, the method of vitrification by rapid freezing was introduced for the preparation of viruses (Adrian *et al.*, 1984) and used for electron crystallographic studies, for example in Unwin and Ennis (1984), Chang *et al.* (1985), Havelka *et al.* (1995), Karrasch *et al.* (1995), Grigorieff *et al.* (1995a), Cheng *et al.* (1997), and Unger *et al.* (1997b). Although, so far, no atomic structure has been determined from vitrified specimens, vitrification keeps the specimen in an aqueous environment closely resembling its natural environment. Thus, vitrification provides the necessary tool for time-resolved electron microscopy, where structural changes accompanying different states in a cycle of molecular functions can be trapped by rapid freezing (Subramaniam *et al.*, 1993, 1997; Berriman and Unwin, 1994; Han *et al.*, 1994*b;* Moffat and Henderson, 1995). Nowadays, sugar embedding and quick freezing are often combined yielding very reproducible results (Nogales *et al.*, 1995; Kimura *et al.*, 1997; Walz *et al.*, 1997*b*). Moreover, new preparation methods are developed such as embedding in cubic ice by controlled devitrification which improves the signal-to-noise ratio and appears to give a higher success rate for high resolution images compared with vitrified samples (Cyrklaff and Kühlbrandt, 1994). Freeze drying (Gross *et al.*, 1990), a preparation technique originally used for metal shadowing, might also play a role for electron crystallography in the future. The major advantage of this method is that the structure is not embedded in sugar or ice which usually contributes to the background noise and lowers the contrast of the protein. The high image contrast might be important for obtaining high-resolution information from very small crystals where only limited averaging for signal-to-noise improvement is possible. Although it is not clear yet whether freeze drying is capable to preserve atomic details of a biological specimen, unpublished results show that a resolution better than 10 Å can be obtained from very small crystalline areas (T. Walz, P. Tittmann, K. Fuchs, H. Gross, and A. Engel, unpublished results).

Preparation of specimens suitable for high resolution electron crystallography must also provide almost perfectly flat specimen areas. Imperfect specimen flatness is a major problem for the recording of images and electron diffraction data at higher tilt angles because it causes spots perpendicular to the tilt axis to be blurred (Glaeser *et al.*, 1991). The lack of specimen flatness is mainly due to the roughness of the carbon film (Butt *et al.*, 1991; Glaeser, 1992*a;* Han *et al.*, 1994*a*), and the difference in the linear thermal expansion coefficient between the amorphous carbon film and the copper grid, leading to "cryo crinkling" when the grid is cooled (Booy and Pawley, 1993; Schmutz and Brisson, 1996). While cryo crinkling can be significantly reduced by the use of molybdenum grids, the preparation of flat carbon support films is still difficult and often nonreproducible. To reduce the beam-induced movement and charging of the specimen (see below), a carbon sandwich technique is under investigation, in which

a thin layer of carbon is evaporated onto the prepared specimen, similar to a technique introduced for specimens which are not supported by a carbon film (Jakubowski *et al.*, 1989)

Data Collection

While high resolution electron diffraction patterns of bR were recorded many years ago (Unwin and Henderson, 1975), the ability to record and extract high resolution phases from images has been more recent (Jeng *et al.*, 1984; Henderson *et al.*, 1986; Baldwin *et al.*, 1988). Several reasons for the deterioration of the image quality have been identified and include radiation damage, beam-induced specimen movement and charging, and attenuation of the envelope function of the phase contrast transfer function (CTF) due to imperfect coherence of the electron beam. The influence of the various effects is discussed in Henderson and Glaeser (1985) and reviewed in Bullough (1990*c*) and Henderson (1992).

Biological specimens are susceptible to radiation damage (Glaeser, 1971), and, therefore, low-dose imaging techniques are now commonly used to limit specimen damage as much as possible (Williams and Fisher, 1970). Further reduction of the effect of beam damage is achieved by cooling the specimen to low temperatures. While cryo-electron microscopy is usually performed at liquid nitrogen temperature reducing the effects of beam damage by a factor of 3 to 5 (International Experimental Study Group, 1986), the work by Fujiyoshi *et al.* (1986) suggests that the cryo-protection can still be improved by a factor of 2 when the specimen is cooled to liquid helium temperature, prompting the development of a superfluid helium stage (Fujiyoshi *et al.*, 1991). Although the effective gain of helium cooling is still under discussion, it is intriguing that the images with the highest resolution were taken by helium-cooled electron microscopes either in Berlin (bR in projection at 2.8 Å by Baldwin *et al.* (1988) and at 2.6 Å by Grigorieff *et al.* (1995*a*)) or in Japan (LHC II in 3-D at 3.4 Å by Kühlbrandt *et al.* (1994) and bR in 3-D at 3.0 Å by Kimura *et al.* (1997)). However, it must be stated that these microscopes are also equipped with top-entry specimen stages which are known to be more stable than the conventional side-entry stages. In addition, the microscope developed by Fujiyoshi *et al.* (1991) provides for very rapid specimen exchange in less than 15 min. This can be important when high-quality specimens are difficult to obtain and, therefore, a large number of specimens has to be inspected before a suitable sample is found.

In the time when electron crystallography was developed, commonly used electron microscopes had an acceleration voltage of about 100 kV and were equipped with a conventional thermionic electron gun. However, these instruments were not ideal for high resolution imaging due to their poor electron-optical performance which is characterized by the rapid attenuation of the envelope of the CTF (see for example Frank (1973)). A modern electron microscope used for high-resolution electron crystallography has an acceleration voltage of 200 kV or more, and/or it is equipped with a field emission gun. Compared with a conventional thermionic gun, a field emission gun produces a beam which has a better spatial coherence due to the higher brightness and smaller effective size of the electron source, and it has a better temporal coherence due to the smaller energy spread. This leads to an improved CTF envelope with a reduced attenuation of the image amplitudes toward higher resolution. While the higher acceleration voltage may also help to reduce beam-induced movement and charging of the specimen, spot-scanning originally suggested by Henderson and Glaeser (1985) proved to be very effective in this respect. Here, the beam is reduced to a small diameter and scanned over the specimen to build up the image (Downing and Glaeser, 1986; Bullough and Henderson, 1987). Spot-scanning produces better images because, at any given time during the build up of the image, only a small area of the specimen is illuminated, thereby reducing beam-induced movement and charging. Details of this method can be found in reviews by Bullough (1990*c*) and Downing (1991). The use of an anticontaminator fork or an objective aperture was also reported to reduce the charge built-up, possibly due to neutralization by secondary electrons ejected from the anticontaminator (Dubochet *et al.*, 1988).

Slow-scan charge-coupled device (SSCCD) cameras were introduced in automated electron tomography where instant access to the acquired data is important (Dierksen *et al.*, 1992; Downing *et al.*, 1992; Koster *et al.*, 1992*a;* Koster and Ruijter, 1992*b;* Dierksen *et al.*, 1993). The use of SSCCD cameras for recording electron diffraction data (Brink and Chiu, 1994) brought a major improvement. SSCCD cameras display excellent recording characteristics in terms of dynamic range, linearity, and background noise (de Ruijter and Weiss, 1992; Krivanek and Mooney, 1993), and, in this respect, they are superior to photographic film. Moreover, the instant access to the acquired data makes immediate evaluation of the data possible. The small field of view of SSCCD cameras (usually 1024×1024 pixels) can be limiting when diffraction patterns are recorded from crystals with large unit cells such as the tropomyosin 2-D crystals (Avila-Sakar *et al.*, 1993), leading to closely spaced diffraction spots which complicate accurate background determination. This problem can be solved by the use of larger chips, for example chips

with a 2K × 2K area, which allow larger camera lengths to be used. However, until SSCCD cameras with a size of 10K × 10K pixels or more are available, photographic film is still the best detector for images, because it provides a larger active area while recording small detail needed to obtain high resolution data. In this case, the film is scanned using a densitometer to obtain a pixel image on the computer.

Image Processing

Usually, electron diffraction patterns are used to extract accurate diffraction amplitudes (which are not affected by CTF modulation and the envelope function or specimen drift), while the phases are determined from the micrographs. Then diffraction patterns and micrographs from several untilted and tilted specimens are processed and averaged to determine a complete 3-D amplitude and phase data set. In the last step, the amplitudes and phases are combined to calculate the final density map. This procedure was first outlined in 1975 (Henderson and Unwin, 1975; Unwin and Henderson, 1975) and later refined in a comprehensive paper in 1982 (Amos *et al*., 1982). Today, several program packages for electron microscopical image analysis are available (reviewed in *J. Struct. Biol.* **116**, No. 1). However, the program suite developed at the MRC in Cambridge (Crowther *et al*., 1996), and programs derived from it, are used for most of the computational analysis of electron crystallographic data.

A description of the procedures involved in the analysis and merging of electron diffraction data is given in Baldwin and Henderson (1984) and Ceska and Henderson (1990), where all the individual processing steps and necessary corrections to obtain a full 3-D amplitude data set are summarized. Amplitudes determined by these procedures were used for the atomic models of bR (Henderson *et al*., 1990) and LHC-II (Kühlbrandt *et al*., 1994). One problem with amplitudes measured from electron diffraction patterns is created by diffraction intensities rendered negative after background subtraction. In the work on bR, which included diffraction patterns from samples tilted up to 60°, the number of such reflections was much higher than theoretically expected from the noise level in the data. The fraction of negative intensities could be significantly reduced by taking into account the background intensity in diffraction patterns arising from diffuse scattering, which could be related to disorder present in purple membrane crystals (Grigorieff and Henderson, 1995*b*). The refinement of the bR model based on the corrected diffraction data was done with programs originally developed for X-ray crystallography, but with modifications necessary to deal with electron diffraction data (Grigorieff *et al*., 1996*a*). The resolution of the bR data set was improved later by Kimura *et al*. (1997), who recorded diffraction patterns up to a tilt angle of 70° on a 1K × 1K SSCCD camera.

In low dose imaging, only about 10 electrons per $Å^2$ build up the image, leading to a very low signal-to-noise ratio in the image. Thus, extensive image processing is required to extract the signal from the background noise. Apart from the Fourier filtration which removes most of the noise, the processing also involves elimination of crystal distortions in an image (unbending), and correction for the CTF. The reader is referred to Amos *et al*. (1982) and Henderson *et al*. (1986) for comprehensive reviews dealing with each of these steps. Whenever possible, electron diffraction amplitudes are used to calculate the final density map. However, many 2-D crystals are too small to record electron diffraction patterns, and, therefore, a scaling procedure was developed for image amplitudes which are usually more strongly attenuated toward higher resolution than diffraction amplitudes (Havelka *et al*., 1995). The key step in this procedure is the application of a negative temperature factor which could be anisotropic. The temperature factor in the image amplitudes is determined by a comparison with a reference data set, for example, with bR electron diffraction intensities. This procedure was used for the 3-D maps of halorhodopsin (Havelka *et al*., 1995) and rhodopsin (Unger and Schertler, 1995; Unger *et al*., 1997b).

Due to the geometry of the experimental set-up, and because of imperfect specimen flatness, it is unrealistic to collect data from specimens which are tilted by much more than 70°. In the case of 2-D crystals, this results in a conical volume of the reciprocal space which cannot be sampled (known as the missing cone). The missing cone leads to a nonisotropic resolution which is lower in the direction perpendicular to the plane of the membrane than in the plane although if data to 60° or 70° tilts are available, the missing cone amounts only to 13 or 6% of the full data, respectively (Glaeser *et al*., 1989b; Glaeser and Downing, 1993). Processing of electron microscopical data is based on the weak phase object (WPO) approximation (Jap and Glaeser, 1980; Cohen *et al*., 1984). However, the large atomic scattering cross-sections for electrons which make the electron crystallographic investigations of thin 2-D crystals possible, lead to multiple (dynamical) scattering (Glaeser and Ceska, 1989a), questioning the validity of the WPO approximation. Glaeser and Downing (1993) studied the magnitude of dynamical scattering for 100 kV electrons and concluded that the effect of dynamical scattering can be neglected for purple membrane crystals and for other crystals

of similar thickness and with equal or larger unit cell dimensions. However, the differences in the Friedel-related reflections, which are due to dynamical scattering and the curvature of the Ewald sphere, could in principle be used to refine structure factor phases (Grigorieff and Henderson, 1996b).

Finally, it is worth mentioning two problems often encountered in electron crystallographic work: the determination of the handedness of a structure, and the measurement of the resolution in a density map. Although there is no theoretical problem to obtain the correct handedness of a low-resolution structure, in practice it appears to be very easy to make a mistake. The ultimate answer is brought only by the high resolution structure, where the main chain can be traced and the handedness of the individual α-helices can be observed. However, the image processing procedure leading to the observed handedness of the structure can be verified by processing a tilted image of a protein with a known structure, for example bR. Alternatively, atomic force microscopy can be used to confirm the surface structure if it is visible. Details of these approaches are described in Heymann *et al.* (1997). The resolution of an image or a density map is commonly defined with the highest resolution spot included in the data processing. However, the effective resolution visible as resolved detail in a map appears often to be lower than this. Using a bR projection map at a nominal resolution of 3.5 Å, Glaeser *et al.* (1992*b*) demonstrated by computer simulations that the loss of visible high resolution detail is due to the attenuated high resolution amplitudes, the sparsity of high resolution data, and the noise present in the data.

STRUCTURES UNDER INVESTIGATION

There follows an overview over the rapidly increasing number of membrane proteins currently investigated by electron crystallography of 2-D crystals which allowed data collection to a resolution better than 10 Å. However, the 3-D structures of many other membrane proteins have been determined at lower resolution, and the reader is referred to articles, for example by Jap *et al.* (1992) and Kühlbrandt (1992).

Bacteriorhodopsin

Bacteriorhodopsin (bR) is a light-driven proton pump in the cell membrane of *Halobacterium salinarium*. The photochemical reactions which underlie proton pumping are manifested as a sequence of photo intermediates which can be observed by their absorption in the visible (for reviews see Mathies *et al.* (1991), Oesterhelt *et al.* (1992), Rothschild (1992), Ebrey (1993) and Lanyi (1993)). The determination of its 3-D structure with data to 7 Å resolution from naturally occuring membrane patches was the first case in which the secondary structure of an integral membrane protein was visualized (Henderson and Unwin, 1975; Unwin and Henderson, 1975). The 3-D structure was subsequently determined to near-atomic resolution (3.5 Å in the plane of the membrane and 7.8 Å perpendicular to it) by electron crystallographic methods, and, using the amino acid sequence of bR (Khorana *et al.*, 1979; Ovchinnikov *et al.*, 1979), an atomic model could be fitted to the map (Henderson *et al.*, 1990). This higher resolution work was helped by the application of electron crystallography to large 2-D crystals of bR, produced by fusing smaller crystals which occur naturally in the bacterial cell membrane (purple membrane). The original atomic model, which was later refined (Grigorieff *et al.*, 1996a), revealed seven transmembrane α-helices and a retinal covalently linked to a lysine via a Schiff base, located approximately in the middle of the membrane (see Fig. 1a). Three of the six surface loops showed only weak density, leaving their structure uncertain. Recently, similar data have been collected using electron crystallography with phases to 3.0 Å resolution, revealing the structure of the three remaining surface loops more clearly (Kimura *et al.*, 1997), see Fig. 1b. This structure has been refined (Mitsuoka *et al.*, submitted).

The chromophore retinal gives the protein its purple color and isomerizes upon absorption of a photon at 568 nm, thereby starting the photocycle which is accompanied by a series of conformational changes. These changes are indicated by approximately 10% changes in the structure factor amplitudes observed by neutron diffraction (Dencher *et al.*, 1989), X-ray diffraction (Koch *et al.*, 1991; Nakasako *et al.*, 1991), and electron diffraction (Subramaniam *et al.*, 1993; Han *et al.*, 1994b; Vonck, 1996; Subramaniam *et al.*, 1997). The Fourier difference maps, calculated using phases obtained by electron crystallography for the bR ground state, suggest that the largest changes occur in the M-intermediate of the photocycle, causing an opening of the cytoplasmic end of the proton channel, presumably to allow proton transfer from the surface to the Schiff base. The next step in the study of the photo intermediates will be the collection of diffraction data at high tilt angles (for example 60°) to obtain high-resolution difference maps for each intermediate in the photocycle. Recently, new methods in crystallization and X-ray diffraction have made it possible to collect data to 2.5 Å resolution from small crystals of bR (Pebay-Peyroula *et al.*, 1997), thus providing another approach to obtain high-resolution structures of the intermediates. If the conformational changes associated with the photo intermediates are not localized to a few domains, but consist of a number of small

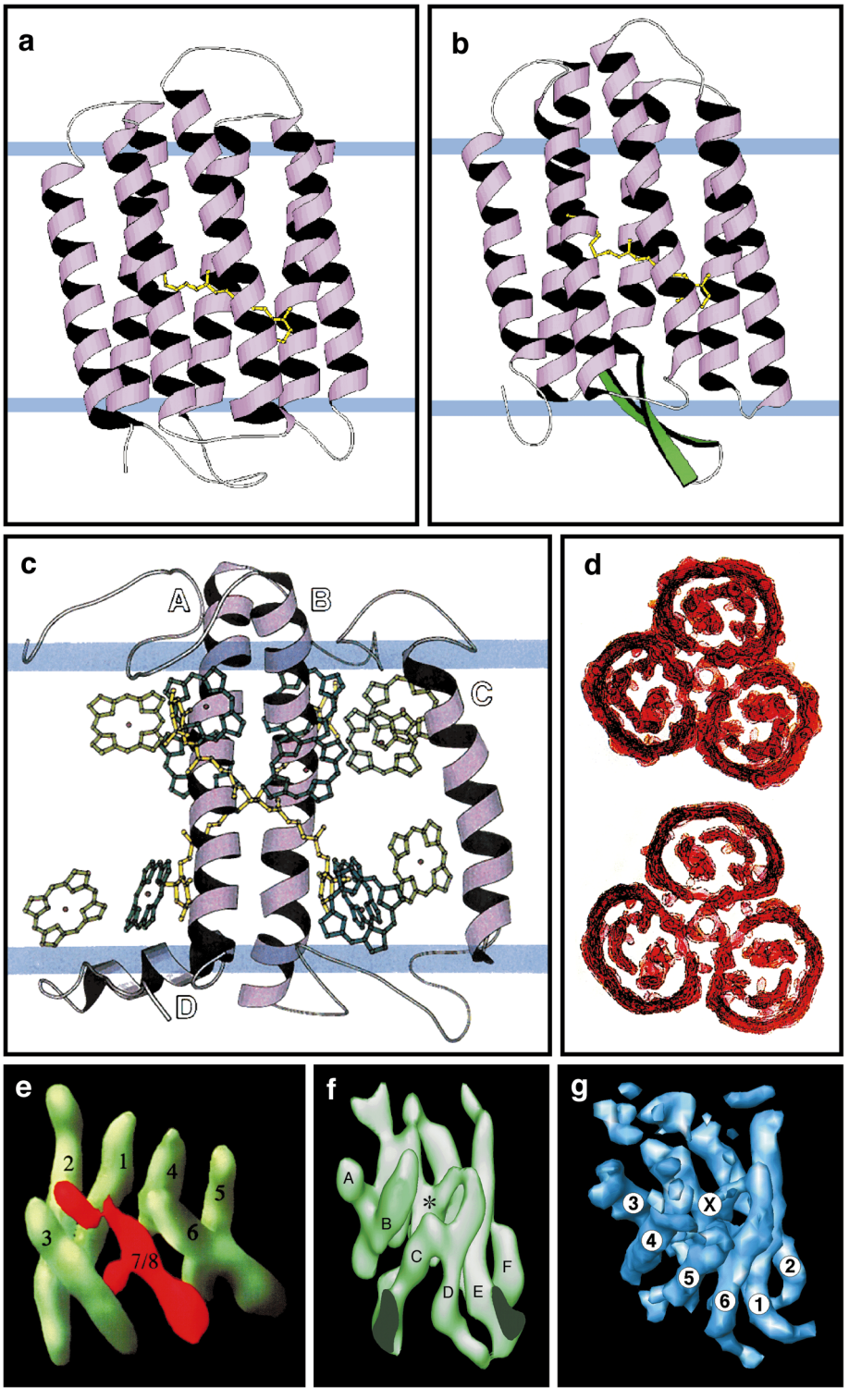

FIG. 1. Three-dimensional structures of several membrane proteins determined by electron crystallography of two-dimensional crystals. (a and b) Ribbon diagrams of two bacteriorhodopsin models created using MOLSCRIPT (Kraulis, 1991). The seven transmembrane helices are drawn in violet and the retinal is shown in yellow. The blue lines indicate the approximate position of the lipid bilayer. The model in (a) represents the refined structure by Grigorieff *et al.* (1996) including data to 3.5 Å resolution. In (b) a more recent model of bR determined by Kimura *et al.* (1997) is shown which includes data to 3.0 Å resolution. In addition to the seven helices, the density map at 3 Å resolution revealed for the first time an antiparallel β-sheet in the BC loop which is shown in light green. (b) This image was kindly prepared by Kaorum Mitsuoka. (c) The ribbon diagram of light-harvesting complex from pea leaves shows the three transmembrane helices (violet), the two lutein molecules (yellow), and 12 bacteriochlorophyll molecules (Chl *a* in light green and Chl *b* in dark green). The

changes in different areas within the protein, the difference Fourier maps require structure factor phases to be obtained from images of the intermediates to allow the distinction to be made between noise and features related to the genuine changes in the structure (Lindahl and Henderson, 1997). However, atomic models can also be refined against 3-D electron diffraction data alone.

Light-Harvesting Complex II from Plants

The light-harvesting complex II (LHC-II) was the second atomic structure of an integral membrane protein to be solved by electron crystallography (Fig. 1c). It is associated with photosystem II for which it functions as an antenna to collect light energy. LHC-II from pea chloroplasts was purified and reconstituted into 2-D crystals with $p32_1$ symmetry. A 3-D density map at 6 Å resolved three membrane-spanning helices and several additional densities which were assigned to chlorophyll porphyrins (Kühlbrandt and Wang, 1991). The density map at 3.4 Å resolution finally resolved about 80% of the polypeptide revealing a small fourth α-helix, 12 (possibly 13) chlorophylls, and 2 carotenoids (Kühlbrandt *et al.*, 1994). While the polypeptide seems mainly involved in ligand binding, the carotenoids appear to have an important structural role by forming an internal cross-brace which provides strong links between peptide loops at both surfaces of the membrane. The atomic model of LHC-II has important implications for the function of the chlorophylls in collection and transfer of light energy and the mechanism of photoprotection by the carotenoids.

Bacterial Porins

Most porins are found in the outer membranes of gram-negative bacteria where they form more or less specific pores (Jap and Walian, 1990b; Schirmer and Rosenbusch, 1991). Porins are often highly abundant and can even form 2-D crystals *in vivo* (Kessel *et al.*, 1988; Rachel *et al.*, 1990). If this is not the case porins can easily be induced to form 2-D crystals (Dorset *et al.*, 1983; Jap, 1988; Lepault *et al.*, 1988). Projection maps of several porins were produced by cryo-electron microscopy (Chang *et al.*, 1985; Sass *et al.*, 1989; Jap *et al.*, 1990*a*), but only PhoE was tilted in the electron microscope to produce a 3-D map at 6 Å resolution (Fig. 1d; Jap *et al.*, 1991). While this resolution is usually sufficient to see membrane-spanning α-helices, it was not enough to resolve the individual, highly tilted β-strands in the porin β-barrel structure. The first atomic model for a porin revealing the 16-stranded antiparallel β-barrel came from X-ray crystallography (Weiss *et al.*, 1990; Weiss and Schulz, 1992) confirming the earlier electron crystallographic work. Although the porin structures are now dominated by X-ray crystallography (Cowan *et al.*, 1992; Schirmer *et al.*, 1995; Hirsch *et al.*, 1997), work continues on well-ordered 2-D crystals using electron crystallography (Simón *et al.*, 1996; Zhuang *et al.*, 1997).

Aquaporin-1

The recently discovered aquaporin-1 (AQP1) (Denker *et al.*, 1988) was the first identified water-specific membrane pore (Preston *et al.*, 1992). The marked propensity of AQP1 to form well-ordered 2-D crystals and the biological importance of the ubiquitous water channels prompted a number of electron crystallographic studies. Three groups produced crystals with adjacent AQP1 tetramers incorporated in the membrane in opposite orientations ($p42_12$ symmetry), and they obtained a projection map below 10 Å. All maps showed a trapezoid-shaped ring of densities forming the border of the monomer; however, only two groups detected a density in the center of the monomer (Jap and Li, 1995; Walz *et al.*, 1995) which was missing in the third projection map (Mitra *et al.*, 1995). More agreement on the AQP1 structure was achieved by determination of the 3-D density maps (Fig. 1e-g; Li *et al.*, 1997; Cheng *et al.*, 1997; Walz *et al.*, 1997b) showing that the monomer is formed by six highly tilted membrane-spanning α-helices surrounding a complex Y-shaped density. Two groups have a right-handed helix bundle (Figs. 1f and 1g; Cheng *et al.*, 1997; Walz *et al.*, 1997*b*), while the third group found a left-handed helix bundle (Fig. 1e; Li *et al.*, 1997). There is strong evidence for the correctness of the unusual right-handed packing of the AQP1 helix bundle (Heymann

blue lines indicate the approximate position of the lipid bilayer. Figure reprinted with permission from *Nature* (Kühlbrandt *et al.*, 1994, Copyright 1994, Macmillan Magazines Limited). (d) Views of stacked serial sections obtained from the 3-D map of the bacterial porin PhoE at 6 Å resolution. The stacked 3-D model of thickness 36 Å is shown as viewed from the extracellular side (top) and from the intracellular side (bottom). Figure reprinted with permission from *Nature* (Jap *et al.*, 1991, Copyright 1991, Macmillan Magazines Limited). (e–g) The three recently determined 3-D density maps of aquaporin-1 (AQP1) all reveal six highly tilted transmembrane helices surrounding a complex structure in the center of the monomer which probably forms the water-specific channel. (d) This image is reprinted with permission from *Nature Structural Biology* (Li *et al.*, 1997, Copyright 1997, Macmillan Magazines Limited), (e) was kindly prepared by Alok Mitra from data published in Cheng *et al.* (1997), and (f) is reprinted with permission from *Nature* (Walz *et al.*, 1997b, Copyright 1997, Macmillan Magazines Limited).

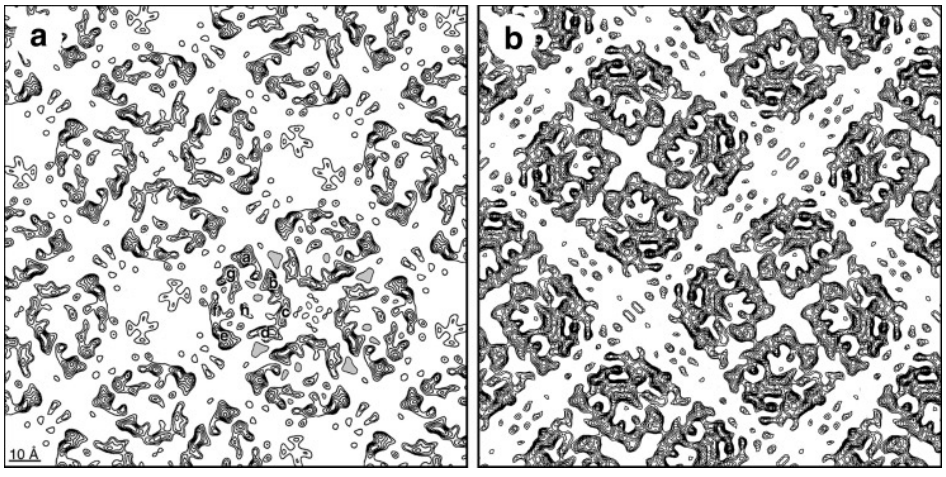

FIG. 2. Projection maps of aquaporin-1 (AQP1). (a and b). The projection maps at 3.5 Å resolution illustrate the high quality of the 2-D AQP1 crystals which should eventually allow the determination of the atomic structure of this highly specific water channel. (a) This image is reprinted with permission from *Journal of Molecular Biology* (Jap and Li, 1995, Copyright 1995 by Academic Press, Inc.), and (b) represents unpublished data by T. Walz, T. Hirai, K. Murata, K. Mitsuoka, Y. Fujiyoshi, and A. Engel.

et al., 1997), but a more definite answer will be brought by a 3-D map at near-atomic resolution. This appears a feasible goal with the current 2-D crystals which allowed determination of projection maps at 3.5 Å resolution (Figs. 2a and 2b).

Halorhodopsin

Halorhodopsin (HR) is a light-driven chloride pump found in the cell membrane of *Halobacterium salinarium* (Schobert and Lanyi, 1982). 2-D crystalline arrays of HR formed spontaneously in the membrane of a HR overexpressing *Halobacterium salinarium* strain (Havelka *et al.*, 1993; Heymann *et al.*, 1993). A projection map at 6 Å resolution revealed a tetrameric assembly of HR in the crystalline patches in contrast to the trimeric assembly of bR in the purple membrane. However, the structure of HR appears to be almost identical to bR at 6 Å resolution. Interestingly, adjacent HR tetramers were found to be in alternate orientations and were related to each other by a screw axis in the membrane plane ($p42_12_1$ symmetry; see Fig. 3a). The presence of additional 14 residues at the N-terminus of the genetically modified HR which included a positively charged histidine residue was suggested as a possible reason for the small fraction of misinserted proteins. Because of the limited size of the crystalline areas, no electron diffraction patterns of tilted specimens could be recorded. Thus, a 3-D structure of HR at 7 Å resolution had to be calculated without using electron diffraction data of tilted specimens (Fig. 3b; Havelka *et al.*, 1995). Again, the 3-D density map of HR is very similar to the 3-D map of bR at that resolution. However, the structure suggests a slightly larger cross-sectional area between the helices B, C, F, and G at the cytoplasmic end of the molecule compared to bR which is needed to accommodate the larger chloride ions. The lower channel surrounded by the helices B, C, G, and A has approximately the same cross-section in HR and bR.

Rhodopsin

Rhodopsin, a G-protein-coupled receptor found in the photoreceptor membranes of the retina, triggers the visual transduction cascade in photoreceptors upon photon absorbtion. The first direct visualization of α-helices in rhodopsin came from a projection map of 2-D crystallized bovine rhodopsin (Schertler *et al.*, 1993). Compared to the somewhat elongated top view of bacteriorhodopsin (Fig. 3c), bovine rhodopsin (Fig. 3d) is rather compact, and the different helix packing is consistent with the structural constraints derived from comparison of over 200 G-protein-coupled receptor sequences (Baldwin, 1993). A low-resolution 3-D density map calculated from image phases and scaled image amplitudes (Unger and Schertler, 1995) resolved four helices. However, the limited tilt angle of only 30° used for imaging was not sufficient to resolve the remaining three helices which appear to be highly tilted to form a continuous arc-shaped feature in the 3-D map of bovine rhodopsin. 2-D arrays of frog rhodopsin (projection map shown in Fig. 3e), crystallized *in situ* by mild detergent treatment of rod cell outer segment disc membranes (Schertler and Hargrave, 1995), displayed a higher crystallinity which resulted in an improved 3-D map where all the α-helices were resolved (Figs. 3g and 3h; Unger *et al.*, 1997b). 2-D crystals were also obtained from a C-terminally truncated rhodopsin from squid (Fig. 3f; Davies *et*

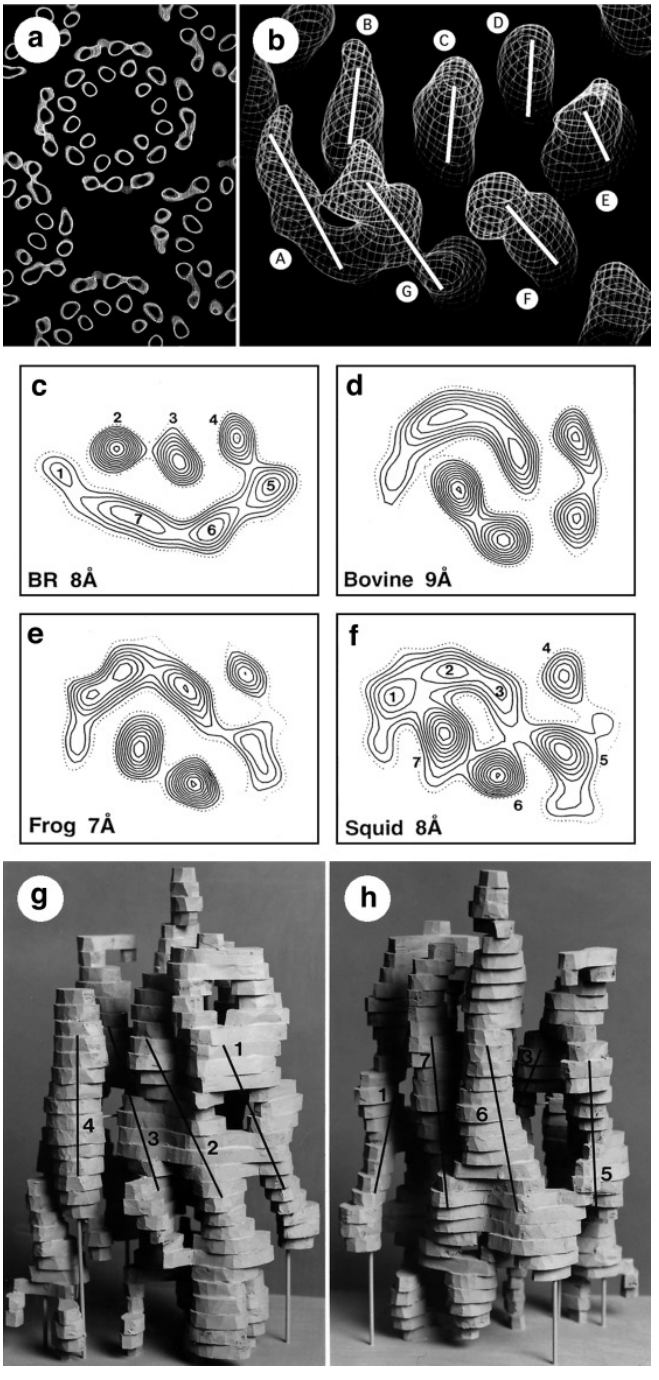

FIG. 3. Electron crystallographic density maps of halorhodopsin and various rhodopsins. (a) The slice of density through the 7 Å 3-D map of halorhodopsin (HR) at about 10 Å from the center of the membrane shows 1 1/2 unit cells with 12 HR molecules in the $p42_12$ crystal lattice. Since alternative tetramers are inverted, this shows in a single view the density corresponding to both sides of the HR molecule. (b) The density corresponding to the helices in one halorhodopsin molecule are visualized by contouring the map at a single density level. The lines drawn into the map represent the tilt of the individual helices. (a and b) These images represent an improved version of Havelka *et al.* (1995), R. Henderson (personal communication). (c) The projection map of bacteriorhodopsin (bR) at 8 Å resolution is shown to illustrate the structural similartity of HR to bR, while the projection maps of rhodopsin from (d) bovine at 9 Å, (e) frog at 7 Å, and (f) squid at 8 Å reveal a different helix packing compared to bR. The helix numbering shown on the squid rhodopsin projection is in accordance with Baldwin (1993). (c to f) These images are reprinted with permission from *Journal of Structural Biology* (Davies *et al.*, 1996, Copyright 1996, Academic Press, Inc). (g and h) Solid representation of the 3-D map of frog rhodopsin showing the membrane-spanning helices. The helices are numbered as in (f) and the lines depict the tilt of the individual helices. Reprinted with permission from *Nature* (Unger *et al.*, 1997b, Copyright 1997, Macmillan Magazines Limited).

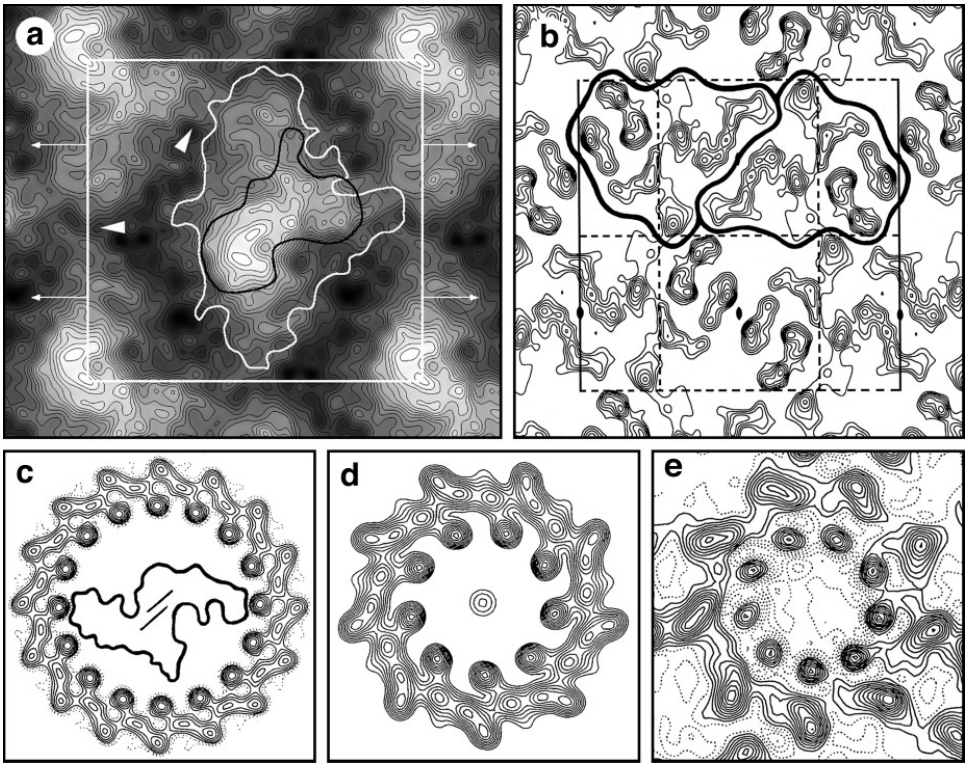

FIG. 4. Electron crystallographic projection maps of membrane proteins involved in photosynthesis. (a) Projection map of the photosystem I (PS I) from *Synechococcus* sp. at 8 Å resolution. The white contour represents the shape of the projected X-ray structure at 6 Å (Krauss *et al.*, 1993) and the black contour indicates the boundary of the stromal protrusion visualised by a 3-D reconstruction of negatively stained PS I 2-D crystals. The unit cell is outlined in white, the arrows indicate the screw axes, and the white arrowheads depict the protein–protein contacts defining the 2-D crystal. Figure reprinted with permission from *Journal of Molecular Biology* (Karrasch *et al.*, 1996, Copyright 1996, Academic Press, Inc). (b) Projection map of photosystem II (PS II) from spinach at 8 Å resolution. The unit cell contains four monomers that are related to eachother by two twofold axes perpendicular to the membrane plane and two twofold screw axes along both a- and b-axis. Two monomers, related by a crystallographic twofold axis, are outlined in bold. Figure reprinted with permission from *Nature* (Rhee *et al.*, 1997, Copyright 1997, Macmillan Magazines Limited). (c) 16-fold rotationally filtered projection map of light-harvesting complex I (LHI) from *Rhodospirillum rubrum* at 8.5 Å resolution. An approximate van der Waals projection of the LM dimer and the single transmembrane α-helix from the H-subunit from the reaction center of *Rhodopseudomonas viridis* (Deisenhofer *et al.*, 1985) has been placed arbitrarily within the LHI ring and the positions of the porphyrin rings of the bacteriochlorophyll *b* special pair is also shown. Figure reprinted with permission from *EMBO Journal* (Karrasch *et al.*, 1995, Copyright 1995, Oxford University Press). (d) Ninefold rotationally filtered projection map of light-harvesting complex II (LHII) from *Rhodovulum sulfidophilum* at 7 Å resolution. Figure reprinted with permission from *Structure* (Savage *et al.*, 1996, Copyright 1996, Current Biology Limited). (e) Projection map of LHII from *Rhodobacter sphaeroides* at 6 Å resolution. The projection map could not be rotationally filtered because the LHII ring is slightly tilted with respect to the membrane plane causing the loss of the ninefold symmetry in projection. Map calculated using data from Walz *et al.*, in preparation.

al., 1996). Despite the phylogenetic distance between squid and vertebrates and the different visual transduction cascades, the rhodopsin projection structures look very similar (compare Figs. 3d and 3e with 3f). The major difference lies in the stronger density peak found for helix 5 in the squid rhodopsin projection map which may be related to the binding site for the Gq class of G-proteins (Hall *et al.*, 1991).

Reaction Centers and Photosystems

Photosynthesis is one of the most fundamental biological reactions which forms the basis for almost all life on earth. Accordingly, countless structural investigations were performed on reaction centers and photosystems, the key complexes in photosynthesis, and the bacterial reaction center from *Rhodopseudomonas viridis* became the first transmembrane protein which was solved to atomic resolution by X-ray crystallography (Deisenhofer *et al.*, 1985, 1995). Although there were also many electron microscopical investigations on photosystem I (PS I) complexes (Fig. 4a), e.g., Ford *et al.* (1990), Böttcher *et al.* (1992), Karrasch *et al.* (1996), X-ray crystallography is most likely to solve its structure as demonstrated by the electron density map at 4 Å resolution (Krauss *et al.*, 1996). X-ray structures for photosystem II (PS II) are not yet available, and electron microsopy is still the only method that can be used for the direct

visualization of its structure (see for example Dekker *et al*. (1990), Holzenburg *et al*. (1993), Santini *et al*. (1994), Marr *et al*. (1996), Nakazato *et al*. (1996), Tsiotis *et al*. (1996), and Morris *et al*. (1997)). Recently, well-ordered PS II 2-D crystals were obtained by dialysis of detergent-solubilized protein and a projection map at 8 Å resolution was calculated (Fig. 4b; Rhee *et al*., 1997). The 2-D crystals are of a high quality and a 3-D density map of PS II below 10 Å can be expected in the near future.

Bacterial Light-Harvesting Complexes

Light-harvesting (LH) complexes of photosynthetic bacteria serve the efficient collection and transfer of light energy to the photosynthetic reaction center (RC). Purple bacteria generally express one or more of three types of light-harvesting complexes referred to as B880 (LHI), B800-850 (LHII), and B800-820 (LHIII) complexes according to their absorption maxima (Cogdell *et al*., 1985). Low resolution studies of intact membranes (Miller, 1982; Stark *et al*., 1984; Engelhardt *et al*., 1986) have shown the bacterial RC to be surrounded by a ring of LHI. Later, the 8.5 Å projection map of LHI from *Rhodospirillum rubrum* (Fig. 4c; Karrasch *et al*., 1995) resolved the individual α-helices of the 16 α,β dimers forming the ring structure. The inner diameter of the LHI ring was shown to be large enough to accomodate an RC *in vivo*. This was supported by low-resolution studies on RC-LHI complexes (Walz and Ghosh, 1997a; Stahlberg *et al*., submitted). However, the apparently closed structure of the LHI ring poses the question on the mechanism of quinone transfer between the RC and the cytochrome bc_1 complex. Two different LHII complexes were solved by X-ray crystallography revealing rings of nine α,β dimers in *Rhodopseudomonas acidophila* (McDermott *et al*., 1995) and eight heterodimers in *Rhodospirillum molischianum* (Koepke *et al*., 1996). Still, it is difficult and time-consuming to crystallize LHII complexes in 3-D to solve their atomic structure. Usually, useful information such as the oligomeric state of LHII complexes can be obtained faster by electron crystallography of 2-D crystals. A projection map at medium resolution can then be compared with the available atomic structures, as demonstrated for *Rhodovulum sulfidophilum* (Fig. 4d; Montoya *et al*., 1995; Savage *et al*., 1996) and for *Rhodobacter sphaeroides* (Fig. 4e; Walz *et al*., in preparation).

Gap Junctions

Gap junction channels, which mediate metabolic and electric coupling of adjacent cells, are formed by a multigene family of gap junction proteins, referred to as connexins (Kumar and Gilula, 1996). The specialized membrane areas where the channels often cluster in a crystalline manner are called gap junction plaques and are characterized by a narrow extracellular gap between the cells. Structural studies of the biologically important gap junctions started very early (Robertson, 1963; Revel and Karnovsky, 1967; Caspar *et al*., 1977). In a 3-D negative stain study, a conformational change was observed after dialysis of isolated gap junction plaques against water for several days (Unwin and Zampighi, 1980), which could also be induced by high calcium concentrations (Unwin, 1983). 3-D reconstructions of the two conformations in ice depicted a tangential tilt of the six subunits forming one hemichannel (connexon) (Unwin and Ennis, 1984) and offered an attractive model for regulating the permeability of membrane channels in general (Unwin, 1986). Further work on gap junctions include 3-D maps in negative stain determined from an invertebrate intercellular communicating junction, which showed an overall structure quite similar to the mammalian gap junction (Sikerwar *et al*., 1991), and from split gap junction plaques (Perkins *et al*., 1997). So far, the highest resolution was obtained from C-terminally truncated recombinant α1 connexin which was expressed in a baby hamster kidney cell line where it formed 2-D crystals *in situ* (Unger *et al*., 1997a). The sixfold symmetrized projection map at 7 Å resolution is shown in Fig. 5a and a 3-D map below 10 Å resolution is currently being determined (V. Unger and M. Yeager, personal communication). For more information on gap junctions the reader is referred to the review by Mark Yeager in this issue.

Plasma Membrane ATPase from Neurospora crassa

The plasma membrane of *Neurospora crassa* contains an H^+-ATPase of the P-type transport ATPase family. Large 2-D crystals of dodecyl maltoside solubilized H^+-ATPase formed on the surface of sitting droplets containing the solubilized protein, a method originally intended for the growth of 3-D crystals (Scarborough, 1994). Due to the missing lipid, the 2-D crystals are fragile and difficult to transfer from the crystallization drop to the electron microscope grid. In the projection map at about 10 Å resolution (Fig. 5b; Cyrklaff *et al*., 1995), the detergent complex of the H^+-ATPase appears as a ring-like hexamer with a complex density distribution. An improved crystallization procedure involves the growth of the 2-D crystals directly on a carbon-coated EM grid where the H^+-ATPase forms thin 3-D crystals. Double-layered crystals displaying a $p32_1$ symmetry were selected to record images of tilted specimens and a 3-D reconstruction at 8 Å resolution is well underway (M. Auer and W. Kühlbrandt, personal communication). Preliminary results clearly resolve the large hydrophilic part and show the arrange-

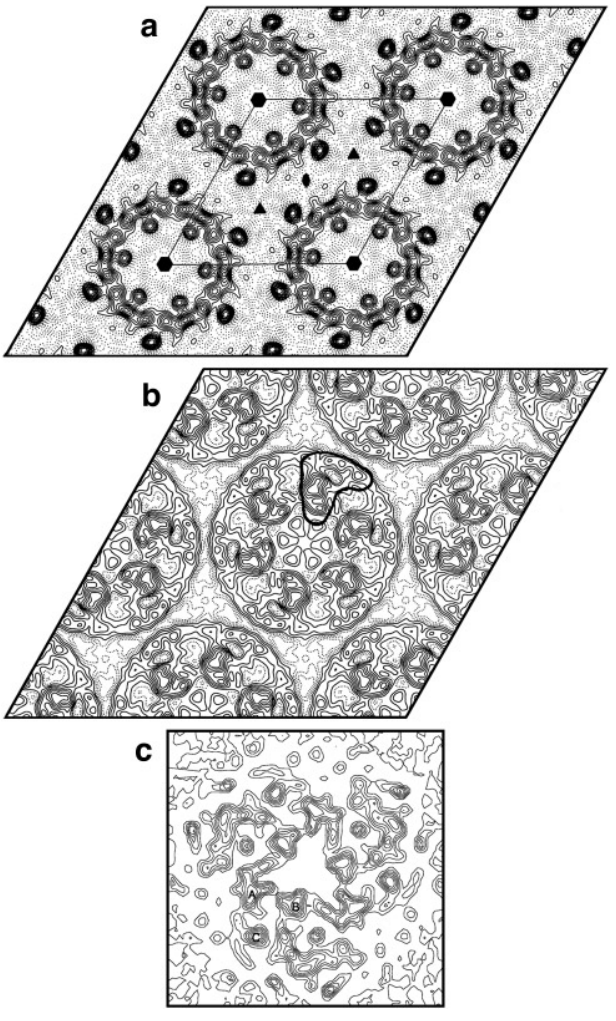

FIG. 5. Projection structures of a gap junction membrane channel, the plasma membrane ATPase from *Neurospora crassa*, and the microsomal glutathione transferase. (a) Sixfold symmetrized projection map of a truncated form of rat heart α_1 connexin at 7 Å resolution. The unit cell is outlined in black and the two-, three-, and sixfold axes are marked with the respective crystallographic symbols. Figure reprinted with permission from *Nature Structural Biology* (Unger *et al.*, 1997a, Copyright 1997, Macmillan Magazines Limited). (b) Sixfold symmetrized projection map of the *Neurospora crassa* plasma membrane ATPase at 10.3 Å resolution. One roughly boot-shaped subunit is oulined in bold. Figure reprinted with permission from *EMBO Journal* (Cyrklaff *et al.*, 1995, Copyright 1995, Oxford University Press). (c) Projection map of the microsomal glutathione transferase trimer at 3 Å resolution after imposing noncrystallographic threefold rotational symmetry. The putative membrane-spanning α-helices are labeled. Figure reprinted by permission from *Journal of Molecular Biology* (Hebert *et al.*, 1997, Copyright 1997, Academic Press, Inc).

ment of the membrane-spanning α-helices (M. Auer and W. Kühlbrandt, personal communication).

Microsomal Glutathione S-Transferase

The microsomal glutathione *S*-transferase (GST) is a transmembrane member of the mostly cytosolic mammalian GSTs, a family of multifunctional enzymes mainly involved in cellular detoxification (Wilce and Parker, 1994). Large well-ordered GST 2-D crystals were formed by dialysis of Triton X-100-solubilized protein in the presence of small amounts of lipid (Hebert *et al.*, 1995). A projection map at 4 Å resolution calculated only from image data showed GST trimers packed on a $p22_12_1$ lattice. The core of the trimer, which is formed by six α-helices running perpendicular to the membrane plane, is surrounded by three elongated domains. An improved projection map at 3 Å resolution includes electron diffraction data and resolves the peripheral domain which now appears to be another α-helix and a complex structure composed of small density maxima with a separation of 4 to 5 Å, which might represent transmembrane β-strands (Hebert *et al.*, 1997). Similar features are observed in a different crystal form which was found at a slightly different lipid-to-protein ratio (Schmidt-Krey *et al.*, in preparation). An atomic 3-D model of the microsomal GST seems feasible and will be required to relate the densities seen in the current projection maps to the known atomic structures of the soluble GSTs (reviewed in Wilce and Parker (1994)) and glutathione binding proteins (Holmgren *et al.*, 1975; Soderberg *et al.*, 1978; Epp *et al.*, 1983).

FUTURE PROSPECTS

2-D crystals have been obtained for many membrane proteins. However, only a few of these have yielded structures at near-atomic resolution in three dimensions. Often, the attainable resolution in electron diffraction patterns is limited due to crystalline disorder or the crystals are too small to record diffraction patterns. A further complication arises with vesicular 2-D crystals which collapse upon adsorption to the EM grid, and which produce two sets of diffraction spots originating from the lower and upper layer of the flattened vesicle. In the images, the two layers can easily be separated by Fourier peak filtration during the processing. However, the accurate determination of amplitudes from electron diffraction patterns is complicated by the additional set of diffraction spots which makes the determination of the background between spots more difficult. Finally, some of the best-diffracting crystals do not consist of a monolayer of molecules, but they are thin 3-D crystals with several layers of ordered protein. In the following some of these problems are discussed.

Thin 3-D Crystals

Some of the best-diffracting crystals suitable for electron crystallography are thin 3-D crystals. The increased thickness leads to stronger multiple scat-

tering of the electrons, which may render the single scattering approximation, assumed for a weak phase object, unsuitable for data analysis, depending on the unit cell size and the crystal thickness. However, using a higher voltage microscope, multiple scattering can be slightly reduced. Apart from the crystallographic symmetry, it is important to find the exact number of layers because the crystal thickness determines the amplitude modulation along the reciprocal lattice lines perpendicular to the membrane plane (Leifer and Henderson, 1983; Shi *et al.*, 1995). The modulation can readily be observed in electron diffraction patterns of tilted thin 3-D crystals. In the case of the H^+-ATPase from *Neurospora crassa* it was relatively easy to select double-layered crystals for imaging (M. Auer, personal communication). However, in most cases it is more difficult and methods have been developed to determine the crystal thickness (Shi *et al*., 1995), so that data from crystals of the same thickness can be merged. The rapid modulation of the Fourier data along the reciprocal lattice lines and the uncertain geometry of stacking (Cheong *et al*., 1996) make the merging more difficult than for single-layered 2-D crystals, and the tilt angle, as well as the tilt axis have to be determined carefully. This is achieved by recording several diffraction patterns from the same crystal at different tilt angles (Brink and Chiu, 1994; Stokes, 1997). The methods currently developed for crotoxin and the Ca^{2+}-ATPase should eventually help to determine the structure of these and other proteins forming thin 3-D crystals (see, for example, Bullough and Tulloch (1990*b*), Grant *et al*. (1991), Taylor and Varga (1994), and Valpuesta *et al*. (1994)).

Small and/or Poorly Ordered 2-D Crystals

Usually, small 2-D crystals and tubular crystals do not allow the recording of high-resolution electron diffraction patterns. Therefore, it would be desirable to calculate a 3-D map at near atomic resolution solely based on image data. With images, the phases are usually measured quite accurately while the amplitudes are significantly attenuated toward higher resolution. The resolution-dependent fall-off can be compensated by scaling the amplitudes against a reference (Havelka *et al.*, 1995). This was done, for example, with data from images of halorhodopsin (Havelka *et al.*, 1995), rhodospin (Schertler *et al.*, 1993; Schertler and Hargrave, 1995), and detergent-treated purple membrane (Grigorieff *et al.*, 1995a). In these cases the reference was provided by diffraction amplitudes of native bR crystals and, therefore, the scaling was biased toward structures with helical bundles. This relatively crude method could be somewhat refined by scaling the amplitudes against X-ray powder diffraction patterns, obtained from the crystals under study, an idea put forward by Wah Chiu (personal communication). Another method currently in use is the scaling of amplitudes by application of a negative temperature factor (Unger and Schertler, 1995; Unger *et al.*, 1997b). Calculation of two projection structures of bR at high resolution (2.6 and 2.8 Å), using scaled image amplitudes in one case and diffraction amplitudes in the other, gave virtually identical results (see Figs. 6a and 6b; Grigorieff *et al.*, 1995a). The possibility of solving a structure to near-atomic resolution with data solely based on images has also been proved theoretically (Henderson, 1995). Thus, even if electron diffraction data are not available, an atomic model for a structure should be possible to obtain from high-resolution image amplitudes and phases. However, future experiments will ultimately show whether this can be done in practice.

In view of the high resolution data which can be extracted from images of 2-D crystals of bR, the question arises why the data are limited to considerably lower resolution in most other cases. Since the resolution degrading factors such as contrast transfer in the microscope, beam damage, and sample movement for all these samples is probably very similar to bR, it is likely that the limited resolution with these other crystals is due to short range disorder, including rotational misalignment, which is not removed by the usual image processing methods. For example, procedures implemented in the MRC program suite (Crowther *et al.*, 1996) only allow translational corrections of small displacements of unit cells from their precise lattice positions, and displacements of individual unit cells or molecules are not detected if the reference area averages over many unit cells. Therefore, to obtain high resolution data from crystals with short range disorder, it is necessary to determine and correct the displacement and rotational misalignment for each molecule or, if several molecules form a rigid complex, for each molecular complex. Methods applied to images of single particles to obtain their 3-D structure are well-suited for this purpose (see for example Frank (1996)), but are usually limited to particles of several hundred kDa. However, the reduced degree of freedom of molecules and molecular complexes in a 2-D crystal should enable their alignment even if their molecular weight is significantly smaller than 100 kDa. This was demonstrated with an image of a 2-D crystal of bR in projection, where the x, y positions of individual bR trimers with a combined molecular weight of about 80 kDa were determined and aligned with the crystal lattice (see Figs. 6c–6e), giving a clear signal at 4 Å resolution in the corrected image (Grigorieff *et al.*, 1995a). The development of more sophisticated image processing methods should

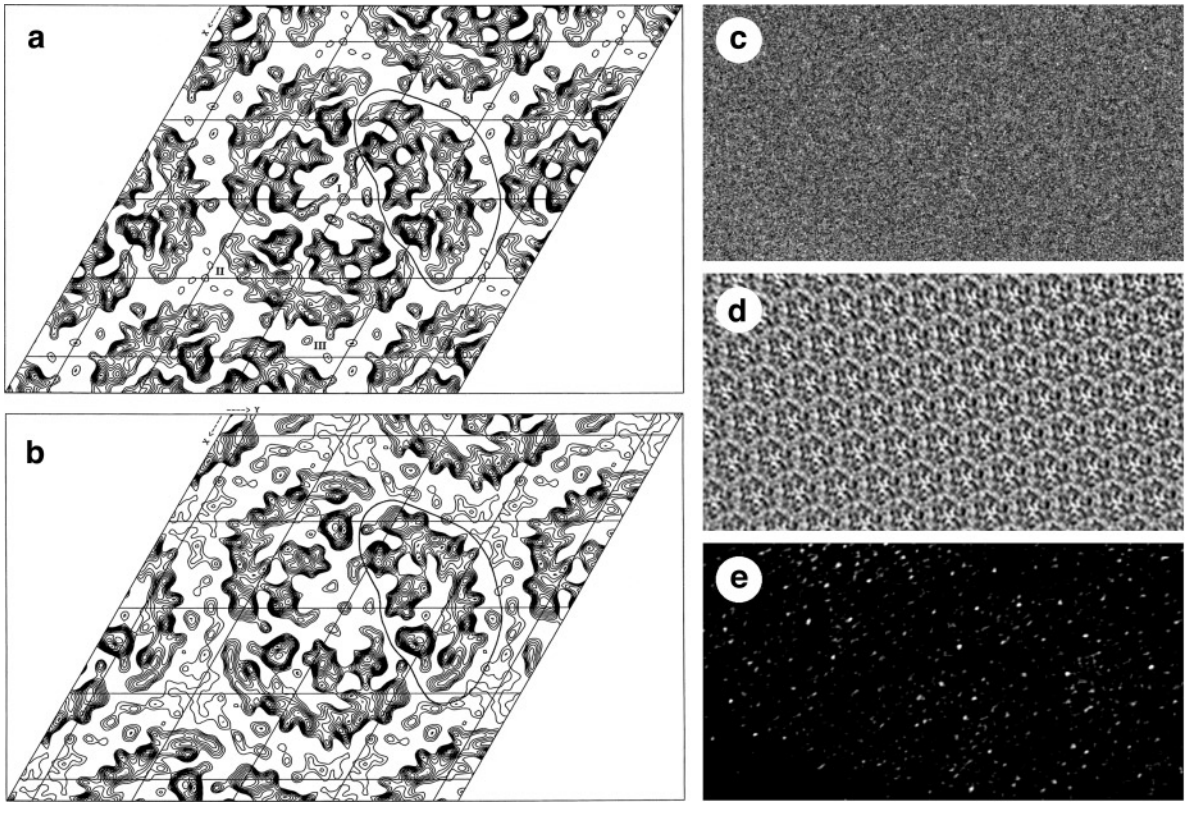

FIG. 6. Scaling of image amplitudes and single-particle treatment of 2-D crystals. (a) Projection map of deoxycholate-treated purple membrane at 2.6 Å resolution. The map was calculated from image amplitudes which were scaled to electron diffraction intensities recorded from native purple membranes. The resulting projection structure of the bR trimers is virtually indistinguishable from the structure of the bR trimers in the projection map of the native purple membrane shown in (*b*), which was calculated using amplitudes extracted from electron diffraction patterns. The threefold axes in (a) are labeled with Roman figures and one bR molecule is outlined in each map. (a and b) These images are reprinted with permission from *Journal of Molecular Biology* (Grigorieff *et al.*, 1995a, Copyright 1995, Academic Press, Inc). (c) A raw image of a 2-D crystal of bR. The signal-to-noise ratio is about 1:8, making it impossible to see individual bR molecules. (d) Fourier-filtered image of (c) revealing the hexagonal 2-D lattice with bR molecules arranged in trimers. (e) Cross-correlation map between the raw image in (c) and a single bR trimer taken from the centre of the filtered image in (d). The correlation peaks with a height of 4– 5 times the standard deviation of the map form a hexagonal lattice, indicating that the x, y positions of individual bR trimers can be detected in the raw image.

also take into account rotational misalignment, and this should include processing of untilted, as well as tilted images. With these new methods electron crystallography and single particle microscopy will merge, making it possible to determine the 3-D structure of biological macromolecules organized in well-ordered crystals, as single particles, and in intermediate configurations (poorly ordered 2-D crystals).

Automation of Data Collection

Automation of the collection of data is already implemented in electron tomography (Dierksen *et al.*, 1992; Downing *et al.*, 1992; Koster *et al.*, 1992a; Koster and Ruijter, 1992b; Dierksen *et al.*, 1993), where limiting the dose is of crucial importance for acquiring many images from the same specimen area (McEwen *et al.*, 1995). So far, little has been achieved with the automation of electron crystallography, although it has the potential of significantly accelerating the data collection process.

We thank P. A. Bullough, A. Engel, H. Hebert, R. Henderson, B. K. Jap, W. Kühlbrandt, A. Mitra, K. Mitsuoka, G. F. X. Schertler, and M. Yeager for providing figures. We are especially grateful to P. A. Bullough, Y. Fujiyoshi, and R. Henderson for many discussions and critical reading of the manuscript. M. Auer, I. Schmidt-Krey, and H. Stahlberg are thanked for discussions on their work and information on yet unpublished results. T.W. wishes to thank EMBO for a postdoctoral fellowship, and N.G. thanks Deutsche Forschungsgemeinschaft for a research fellowship.

REFERENCES

Adrian, M., Dubochet, J., Lepault, J., and McDowall, A. W. (1984) Cryo-electron microscopy of viruses, *Nature* **308,** 32–36.

Amos, L. A., Henderson, R., and Unwin, P. N. T. (1982) Three-dimensional structure determination by electron microscopy of two-dimensional crystals, *Prog. Biophys. Mol. Biol.* **39,** 183–231.

Avila-Sakar, A. J., Schmid, M. F., Li, L. S., Whitby, F., Phillips,

G. N., Jr., and Chiu, W. (1993) Preliminary electron crystallographic analysis of ice-embedded tropomyosin crystals, *J. Struct. Biol.* **110,** 67–74.

Baker, T. S., and Johnson, J. E. (1996) Low-resolution meets high - towards a resolution continuum from cells to atoms, *Curr. Opin. Struct. Biol.* **6,** 585–594.

Baldwin, J., and Henderson, R. (1984) Measurement and evaluation of electron diffraction patterns from two-dimensional crystals, *Ultramicroscopy* **14,** 319–336.

Baldwin, J. M. (1993) The probable arrangement of the helices in G-protein coupled receptors, *EMBO J.* **12,** 1693–1703.

Baldwin, J. M., Henderson, R., Beckmann, E., and Zemlin, F. (1988) Images of purple membrane at 2.8 Å resolution obtained by cryo-electron microscopy, *J. Mol. Biol.* **202,** 585–591.

Berriman, J., and Unwin, N. (1994) Analysis of transient structures by cryo-microscopy combined with rapid mixing of spray droplets, *Ultramicroscopy* **56,** 241–252.

Booy, F. P., and Pawley, J. B. (1993) Cryo-crinkling: what happens to carbon films on copper grids at low temperature, *Ultramicroscopy* **48,** 273–280.

Böttcher, B., Gräber, P., and Boekema, E. J. (1992) The structure of photosystem I from the thermophilic cyanobacterium *Synechococcus* sp. determined by electron microscopy of two-dimensional crystals, *Biochim. Biophys. Acta* **1100,** 125–136.

Böttcher, B., Wynne, S. A., and Crowther, R. A. (1997) Determination of the fold of the core protein of hepatitis B virus by electron cryomicroscopy, *Nature* **386,** 88–91.

Brink, J., and Chiu, W. (1994) Applications of a slow-scan CCD camera in protein electron crystallography, *J. Struct. Biol.* **113,** 23–34.

Bullough, P. A., and Henderson, R. (1987) Use of spot-scan procedure for recording low-dose micrographs of beam-sensitive specimens, *Ultramicroscopy* **21,** 223–229.

Bullough, P. A., and Henderson, R. (1990a) Phase accuracy in high-resolution electron-microscopy of trigonal and orthorhombic purple membrane, *Biophys. J.* **58,** 705–711.

Bullough, P. A., and Tulloch, P. A. (1990b) High-resolution spot-scan electron-microscopy of microcrystals of an alpha-helical coiled-coil protein, *J. Mol. Biol.* **215,** 161–173.

Bullough, P. A. (1990c) Imaging of protein molecules - towards atomic resolution, *Electron Microsc. Rev.* **3,** 249–267.

Butt, H.-J., Wang, D. N., Hansma, P. K., and Kühlbrandt, W. (1991) Effect of surface-roughness of carbon support films on high-resolution electron-diffraction of 2-dimensional protein crystals, *Ultramicroscopy* **36,** 307–318.

Caspar, D. L. D., Goodenough, D. A., Makowski, L., and Phillips, W. C. (1977) Gap juction structures. I. Correlated electron microscopy and X-ray diffraction, *J. Cell Biol.* **74,** 605–628.

Ceska, T. A., and Henderson, R. (1990) Analysis of high-resolution electron-diffraction patterns from purple membrane labeled with heavy-atoms, *J. Mol. Biol.* **213,** 539–560.

Chang, C.-F., Mizushima, S., and Glaeser, R. M. (1985) Projected structure of the pore-forming OmpC protein from *Escherichia coli* outer membrane, *Biophys. J.* **47,** 629–639.

Cheng, A., van Hoek, A. N., Yeager, M., Verkman, A. S., and Mitra, A. K. (1997) Three-dimensional organization of a human water channel, *Nature* **387,** 627–630.

Cheong, G.-W., Young, H. S., Ogawa, H., Toyoshima, C., and Stokes, D. L. (1996) Lamellar stacking in three-dimensional crystals of Ca^{2+}-ATPase from sarcoplasmatic reticulum, *Biophys. J.* **70,** 1689–1699.

Chiu, W. (1993) What does electron cryomicroscopy provide that X-ray crystallography and NMR spectroscopy cannot?, *Annu. Rev. Biophys. Biomol. Struct.* **22,** 233–255.

Chiu, W., and Smith, T. J. (1994) Structural studies of virus-antibody complexes by electron cryomicroscpy and X-ray crystallography, *Curr. Opin. Struct. Biol.* **4,** 219–224.

Cogdell, R. J., Zuber, H., Thornber, J. P., Drews, G., Gingras, G., Niederman, R. A., Parson, W. W., and Feher, G. (1985) Recommendations for the naming of photochemical-reaction centers and light-harvesting pigment-protein complexes from purple photosynthetic bacteria, *Biochim. Biophys. Acta* **806,** 185–186.

Cohen, H., Schmid, M. F., and Chiu, W. (1984) Estimates of validity of projection approximation for three-dimensional reconstructions at high resolution, *Ultramicroscopy* **14,** 219–226.

Conway, J. F., Cheng, N., Zlotnick, A., Wingfield, P. T., Stahl, S. J., and Steven, A. C. (1997) Visualization of a 4-helix bundle in the hepatitis B virus capsid by cryo-electron microscopy, *Nature* **386,** 91–94.

Cowan, S. W., Schirmer, T., Rummel, G., Steiert, M., Ghosh, R., Pauptit, R. A., Jansonius, J. N., and Rosenbusch, J. P. (1992) Crystal structures explain functional properties of two *E. coli* porins, *Nature* **358,** 727–733.

Crowther, R. A., Henderson, R., and Smith, J. M. (1996) MRC image processing programs, *J. Struct. Biol.* **116,** 9–16.

Cyrklaff, M., and Kühlbrandt, W. (1994) High-resolution electron microscopy of biological specimens in cubic ice, *Ultramicroscopy* **55,** 141–153.

Cyrklaff, M., Auer, M., Kühlbrandt, W., and Scarborough, G. A. (1995) 2-D structure of the Neurosporra crassa plasma membrane ATPase as determined by electron cryomicroscopy, *EMBO J.* **14,** 1854–1857.

Davies, A., Schertler, G. F. X., Gowen, B. E., and Saibil, H. R. (1996) Projection structure of an invertebrate rhodopsin, *J. Struct. Biol.* **117,** 36–44.

de Ruijter, W. J., and Weiss, J. K. (1992) Methods to measure properties of slow-scan CCD cameras for electron detection, *Rev. Sci. Instrum.* **63,** 4314–4321.

Deisenhofer, J., Epp, O., Miki, K., Huber, R., and Michel, H. (1985) X-ray structure analysis at 3 Å resolution of a membrane protein complex: folding of the protein subunits in the photosynthetic reaction centre from *Rhodopseudomonas viridis*, *Nature* **318,** 618–624.

Deisenhofer, J., Epp, O., Sinning, I., and Michel, H. (1995) Crystallographic refinement at 2.3-Angstrom resolution and refined model of the photosynthetic reaction-center from *Rhodopseudomonas viridis*, *J. Mol. Biol.* **246,** 429–457.

Dekker, J. P., Betts, S. D., Yocum, C. F., and Boekema, E. (1990) Characterization by electron microscopy of isolated particles and two-dimensional crystals of the CP47-D1-D2-cytochrome b-559 complex of photosystem II, *Biochemistry* **29,** 3220–3225.

Dencher, N. A., Dresselhaus, D., Zaccai, G., and Büldt, G. (1989) Structural changes in bacteriorhodopsin during proton translocation revealed by neutron diffraction, *Proc. Natl. Acad. Sci. USA* **86,** 7876–7879.

Denker, B. M., Smith, B. L., Kuhajda, F. P., and Agre, P. (1988) Identification, purification, and partial characterization of a novel *M*r 28,000 integral membrane protein from erythrocytes and renal tubules, *J. Biol. Chem.* **263,** 15634–15642.

Dierksen, K., Typke, D., Hegerl, R., Koster, A. J., and Baumeister, W. (1992) Towards automatic electron tomography, *Ultramicroscopy* **40,** 71–87.

Dierksen, K., Typke, D., Hegerl, R., and Baumeister, W. (1993) Towards automatic electron tomography. II. Implementation of autofocus and low-dose procedures, *Ultramicroscopy* **49,** 109–120.

Dorset, D. L., Engel, A., Häner, M., Massalski, A., and Rosenbusch, J. P. (1983) Two-dimensional crystal packing of matrix

porin - a channel forming protein in *Escherichia coli* outer membranes, *J. Mol. Biol.* **165,** 701–710.

Downing, K. H., and Glaeser, R. M. (1986) Improvement in high-resolution image quality of radiation-sensitive specimens achieved with reduced spot size of the electron-beam, *Ultramicroscopy* **20,** 269–278.

Downing, K. H. (1991) Spot-scan imaging in transmission electron microscopy, *Science* **251,** 53–59.

Downing, K. H., Koster, A. J., and Typke, D. (1992) Overview of computer-aided electron microscopy, *Ultramicroscopy* **46,** 189–198.

Dubochet, J., Adrian, M., Chang, J.-J., Homo, J.-C., Lepault, J., McDowall, A. W., and Schultz, P. (1988) Cryo-electron microscopy of vitrified specimens, *Q. Rev. Biophys.* **21,** 129–228.

Ebrey, T. G. (1993) Light energy transduction in bacteriorhodopsin, *in* Jackson, M. B. (Ed.), Thermodynamics of Membrane Receptors and Channels, pp. 353–387, CRC Press, Boca Raton.

Engel, A., Hoenger, A., Hefti, A., Henn, C., Ford, R. C., Kistler, J., and Zulauf, M. (1992) Assembly of 2-D membrane protein crystals: dynamics, crystal order, and fidelity of structure analysis by electron microscopy, *J. Struct. Biol.* **109,** 219–234.

Engelhardt, H., Engel, A., and Baumeister, W. (1986) Stoichiometric model of the photosynthetic unit of *Ectothiorhodospira halochloris*, *Proc. Natl. Acad. Sci. USA* **83,** 8972–8976.

Epp, O., Ladenstein, R., and Wendel, A. (1983) The refined structure of the selenoenzyme glutathione peroxidase at 0.2-nm resolution, *Eur. J. Biochem.* **133,** 51–69.

Ford, R. C., Hefti, A., and Engel, A. (1990) Ordered arrays of photosystem I reaction centre after reconstitution: projections and surface reliefs of the complex at 2 nm resolution, *EMBO J.* **9,** 3067–3075.

Frank, J. (1973) The envelope of electron microscopic transfer functions for partially coherent illumination, *Optik* **38,** 519–536.

Frank, J. (1996) Three-dimensional electron microscopy of macromolecular assemblies, Academic Press, San Diego.

Fujiyoshi, Y., Uyeda, N., Yamagishi, H., Morikawa, K., Mizusaki, T., Aoki, Y., Kihara, H., and Harada, Y. (1986) Biological macromolecules observed with high resolution cryo-electron microscope, *in* Proc. XIth Int. Cong. on Electron Microscopy, Vol. 3, pp. 1829, Kyoto.

Fujiyoshi, Y., Mizusaki, T., Morikawa, K., Yamagishi, H., Aoki, Y., Kihara, H., and Harada, Y. (1991) Development of a superfluid helium stage for high-resolution electron microscopy, *Ultramicroscopy* **38,** 241–251.

Fung, J. C., Liu, W. P., de Ruitjter, W. J., Chen, H., Abbey, C. K., Sedat, J. W., and Agard, D. A. (1996) Toward fully automated high-resolution electron tomography, *J. Struct. Biol.* **116,** 181–189.

Glaeser, R. M. (1971) Limitations to significant information in biological electron microscopy as a result of radiation dammage, *J. Ultrastruct. Res.* **36,** 466–482.

Glaeser, R. M., and Ceska, T. A. (1989a) High-voltage electron-diffraction from bacteriorhodopsin (purple membrane) is measurably dynamical, *Acta Crystallogr.* **A45,** 620–628.

Glaeser, R. M., Tong, L., and Kim, S.-H. (1989b) 3-dimensional reconstructions from incomplete data - interpretability of density maps at atomic resolution, *Ultramicroscopy* **27,** 307–318.

Glaeser, R. M., Zilker, A., Radermacher, M., Gaub, H. E., Hartmann, T., and Baumeister, W. (1991) Interfacial energies and surface-tension forces involved in the preparation of thin, flat crystals of biological macromolecules for high-resolution electron-microscopy, *J. Microsc.* **161,** 21–27.

Glaeser, R. M. (1992a) Specimen flatness of thin crystalline arrays - influence of the substrate, *Ultramicroscopy* **46,** 33–43.

Glaeser, R. M., and Downing, K. H. (1992b) Assessment of resolution in biological electron crystallography, *Ultramicroscopy* **47,** 256–265.

Glaeser, R. M., and Downing, K. H. (1993) High-resolution electron crystallography of protein molecules, *Ultramicroscopy* **52,** 478–486.

Grant, R. A., Schmid, M. F., and Chiu, W. (1991) Analysis of symmetry and three-dimensional reconstruction of thin gp32*I crystals, *J. Mol. Biol.* **217,** 551–562.

Grigorieff, N., Beckmann, E., and Zemlin, F. (1995a) Lipid location in deoxycholate-treated purple membrane at 2.6 Ångstroem, *J. Mol. Biol.* **254,** 404–415.

Grigorieff, N., and Henderson, R. (1995b) Diffuse-scattering in electron-diffraction data from protein crystals, *Ultramicroscopy* **60,** 295–309.

Grigorieff, N., Ceska, T. A., Downing, K. H., Baldwin, J. M., and Henderson, R. (1996a) Electron-crystallographic refinement of the structure of bacteriorhodopsin, *J. Mol. Biol.* **259,** 393–421.

Grigorieff, N., and Henderson, R. (1996b) Comparison of calculated and observed dynamical diffraction from purple membrane - implications, *Ultramicroscopy* **65,** 101–107.

Gross, H., Krusche, K., and Tittmann, P. (1990) Recent progress in high-resolution shadowing for biological transmission electron microscopy, *in* Proceedings of the XIIth International Congress for Electron Microscopy, Seattle, San Francisco Press Inc., San Francisco, CA.

International Experimental Study Group (1986) Cryoprotection in electron microscopy, *J. Microsc.* **141,** 385–391.

Hall, M. D., Hoon, M. A., Ryba, N. J. P., Pottinger, J. D. D., Keen, J. N., Saibil, H. R., and Findlay, J. B. C. (1991) Molecular cloning and primary structure of squid (*Loligo forbesi*) rhodopsin, a phospholipase C-directed G-protein-linked receptor, *Biochem. J.* **274,** 35–40.

Han, B.-G., Wolf, S. G., Vonck, J., and Glaeser, R. M. (1994a) Specimen flatness of glucose-embedded biological materials for electron crystallography is affected significantly by the choice of carbon evaporation stock, *Ultramicroscopy* **55,** 1–5.

Han, B. G., Vonck, J., and Glaeser, R. M. (1994b) The bacteriorhodopsin photocycle - direct structural study of 2 substrates of the M-intermediate, *Biophys. J.* **67,** 1179–1186.

Havelka, W. A., Henderson, R., Heymann, A. W., and Oesterhelt, D. (1993) Projection structure of halorhodopsin from *Halobacterium halobium* at 6 Å resolution obtained by electron cryomicroscopy, *J. Mol. Biol.* **234,** 837–846.

Havelka, W. A., Henderson, R., and Oesterhelt, D. (1995) Three-dimensional structure of halorhodopsin at 7 Å resolution, *J. Mol. Biol.* **247,** 726–738.

Hebert, H., Schmidt-Krey, I., and Morgenstern, R. (1995) The projection structure of microsomal glutathione transferase, *EMBO J.* **14,** 3864–3869.

Hebert, H., Schmidt-Krey, I., Morgenstern, R., Murata, K., Hirai, T., Mitsuoka, K., and Fujiyoshi, Y. (1997) The 3.0 Å projection structure of microsomal glutathione transferase as determined by electron crystallography of p21212 two-dimensional crystals, *J. Mol. Biol.* **271,** 751–758.

Henderson, R., and Unwin, P. N. T. (1975) Three-dimensional model of purple membrane obtained by electron microscopy, *Nature* **257,** 28–32.

Henderson, R., and Glaeser, R. M. (1985) Quantitative analysis of image contrast in electron-micrographs of beam-sensitive crystals, *Ultramicroscopy* **16,** 139–150.

Henderson, R., Baldwin, J. M., Downing, K. H., Lepault, J., and Zemlin, F. (1986) Structure of purple membrane from *Halobacterium halobium*: recording, measurement and evaluation of

electron micrographs at 3.5 Å resolution, *Ultramicroscopy* **19,** 147–178.

Henderson, R., Baldwin, J. M., Ceska, T. A., Zemlin, F., Beckmann, E., and Downing, K. H. (1990) Model for the structure of bacteriorhodopsin based on high-resolution electron cryomicroscopy, *J. Mol. Biol.* **213,** 899–929.

Henderson, R. (1992) Image contrast in high-resolution electron microscopy of biological macromolecules: TMV in ice, *Ultramicroscopy* **46,** 1–18.

Henderson, R. (1995) The potential and limitations of neutrons, electrons and X-rays for atomic-resolution microscopy of unstained biological molecules, *Quart. Rev. Biophys.* **28,** 171–193.

Heymann, J. A. W., Havelka, W. A., and Oesterheldt, D. (1993) Homologous overexpression of a light-driven anion pump in an archaebacterium, *Mol. Microbiol.* **7,** 623–630.

Heymann, J. B., Müller, D. J., Mitsuoka, K., and Engel, A. (1997) Electron and atomic force microscopy of membrane proteins, *Curr. Opin. Struct. Biol.* **7,** 543–549.

Hirsch, A., Breed, J., Saxena, K., Richter, O.-M. H., Ludwig, B., Diederichs, K., and Welte, W. (1997) The structure of porin from *Paracoccus denitrificans* at 3.1 Å resolution, *FEBS Lett.* **404,** 208–210.

Holmgren, A., Soderberg, B.-O., Eklund, H., and Branden, C.-I. (1975) Three-dimensional structure of *Escherichia coli* thioredoxin-S2 to 2.8 Å resolution, *Proc. Natl. Acad. Sci. USA* **72,** 2305–2309.

Holzenburg, A., Bewly, M. C., Wilson, F. H., Nicholson, W. V., and Ford, R. C. (1993) Three-dimensional structure of photosystem II, *Nature* **363,** 470–472.

Jakubowski, U., Baumeister, W., and Glaeser, R. M. (1989) Evaporated carbon stabilizes thin, frozen-hydrated specimens, *Ultramicroscopy* **31,** 351–356.

Jap, B. K., and Glaeser, R. M. (1980) The scattering of high-energy electrons. II. Quantitative validity domains of the single-scattering approximations for organic crystals, *Acta Crystallogr.* **A36,** 57–67.

Jap, B. K. (1988) High-resolution electron diffraction of reconstituted PhoE porin, *J. Mol. Biol.* **199,** 229–231.

Jap, B. K., Downing, K. H., and Walian, P. J. (1990a) Structure of PhoE porin in projection at 3.5 Å resolution, *J. Struct. Biol.* **103,** 57–63.

Jap, B. K., and Walian, P. J. (1990b) Biophysics of the structure and function of porins, *Q. Rev. Biophys.* **23,** 367–403.

Jap, B. K., Walian, P. J., and Gehring, K. (1991) Structural architecture of an outer membrane channel as determined by electron crystallography, *Nature* **350,** 167–170.

Jap, B. K., Zulauf, M., Scheybani, T., Hefti, A., Baumeister, W., Aebi, U., and Engel, A. (1992) 2D crystallization: from art to science, *Ultramicroscopy* **46,** 45–84.

Jap, B. K., and Li, H. (1995) Structure of the osmo-regulated H_2O-channel, AQP-CHIP, in projection at 3.5 Å resolution, *J. Mol. Biol.* **251,** 413–420.

Jeng, T.-W., Chiu, W., Zemlin, F., and Zeitler, E. (1984) Electron imaging of crotoxin complex thin crystals at 3.5 Å, *J. Mol. Biol.* **175,** 93–97.

Karrasch, S., Bullough, P. A., and Ghosh, R. (1995) The 8.5 Å projection map of the light-harvesting complex I from *Rhodospirillum rubrum* reveals a ring composed of 16 subunits, *EMBO J.* **14,** 631–638.

Karrasch, S., Typke, D., Walz, T., Miller, M., Tsiotis, G., and Engel, A. (1996) Highly ordered two-dimensional crystals of photosystem I reaction center from *Synechococcus sp.*: functional and structural analyses, *J. Mol. Biol.* **262,** 336–348.

Kessel, M., Brennan, M. J., Trus, B. L., Bisher, M. E., and Steven, A. C. (1988) Naturally crystalline porin in the outer membrane of *Bordetella pertussis*, *J. Mol. Biol.* **203,** 275–278.

Khorana, H. G., Gerber, G. E., Herlihy, W. C., Gray, C. P., anderegg, R. J., Nihei, K., and Biemann, K. (1979) Amino acid sequence of bacteriorhodopsin, *Proc. Natl. Acad. Sci. USA* **76,** 5046–5050.

Kimura, Y., Vassylyev, D. G., Miyazawa, A., Kidera, A., Matsushima, M., Mitsuoka, K., Murata, K., Hirai, T., and Fujiyoshi, Y. (1997) Surface structure of bacteriorhodopsin revealed by high resolution electron crystallography, *Nature* **389,** 206–211.

Koch, M. H. J., Dencher, N. A., Oesterhelt, D., Plöhn, H.-J., Rapp, G., and Büldt, G. (1991) Time-resolved X-ray diffraction study of structural changes associated with the photocycle of bacteriorhodopsin, *EMBO J.* **10,** 521–526.

Koepke, J., Hu, X., Muenke, C., Schulten, K., and Michel, H. (1996) The crystal structure of the light-harvesting complex II (B800–850) from *Rhodospirillum molischianum*, *Structure* **4,** 581–597.

Koster, A. J., Chen, H., Sedat, J. W., and Agard, D. A. (1992a) Automated microscopy for electron tomography, *Ultramicroscopy* **46,** 207–228.

Koster, A. J., and Ruijter, W. J. (1992b) Practical autoalignment of transmission electron microscopes, *Ultramicroscopy* **46,** 189–197.

Kraulis, P. J. (1991) MOLSCRIPT: a program to produce both detailed and schematic plots of protein structures, *J. Appl. Crystallogr.* **24,** 946–950.

Krauss, N., Hinrichs, W., Witt, I., Fromme, P., Pritzkow, W., Dauter, Z., Betzel, C., Wilson, K. S., Witt, H. T., and Saenger, W. (1993) 3-dimensional structure of system-I of photosynthesis at 6 Å resolution, *Nature* **361,** 326–331.

Krauss, N., Schubert, W.-D., Klukas, O., Fromme, P., Witt, H. T., and Saenger, W. (1996) Photosystem I at 4 Å resolution represents the first structural model of a joint photosynthetic reaction centre and core antenna system, *Nature Struct. Biol.* **3,** 965–973.

Krivanek, O. L., and Mooney, P. E. (1993) Applications of slow-scan CCD cameras in transmission electron microscopy, *Ultramicroscopy* **49,** 95–108.

Kühlbrandt, W., and Wang, D. N. (1991) Three-dimensional structure of plant light-harvesting complex determined by electron crystallography, *Nature* **350,** 130–134.

Kühlbrandt, W. (1992) Two-dimensional crystallization of membrane proteins, *Quart. Rev. Biophys.* **25,** 1–49.

Kühlbrandt, W., Wang, D. N., and Fujiyoshi, Y. (1994) Atomic model of plant light-harvesting complex by electron crystallography, *Nature* **367,** 614–621.

Kumar, N. M., and Gilula, N. B. (1996) The gap junction communication channel, *Cell* **84,** 381–388.

Ladinsky, M. S., Kremer, J. R., Furcinitti, P. S., Mcintosh, J. R., and Howell, K. E. (1994) HVEM tomography of the trans-Golgi network - structural insights and identification of a lace-like vesicle coat, *J. Cell Biol.* **127,** 29–38.

Lanyi, J. K. (1993) Proton translocation mechanism and energetics in the light-driven pump bacteriorhodopsin, *Biochim. Biophys. Acta* **1183,** 241–261.

Leifer, D., and Henderson, R. (1983) Three-dimensional structure of orthorhombic purple membrane at 6.5 Å resolution, *J. Mol. Biol.* **163,** 451–466.

Lepault, J., Dargent, B., Tichelaar, W., Rosenbusch, J. P., Leonard, K., and Pattus, F. (1988) Three-dimensional reconstruction of maltoporin from electron microscopy and image processing, *EMBO J.* **7,** 261–268.

Li, H., Lee, S., and Jap, B. K. (1997) Molecular design of

aquaporin-1 water channel as revealed by electron crystallography, *Nature Struct. Biol.* **4,** 263–265.

Lindahl, M., and Henderson, R. (1997) Structure of the bacteriorhodospin D85N/D96N double mutant showing substantial structural changes and a highly twinned, disordered lattice, *Ultramicroscopy*, in press.

Marr, K. M., Mastronarde, D. M., and Lyon, M. K. (1996) Two-dimensional crystals of photosystem II: biochemical characterization, cryoelectron microscopy and localization of the D1 and cytochrome b559, *J. Cell Biol.* **132,** 823–833.

Mathies, R. A., Lin, S. W., Ames, J. B., and Pollard, W. T. (1991) From femtoseconds to biology: Mechanism of bacteriorhodopsin's light-driven proton pump, *Annu. Rev. Biophys. Biophys. Chem.* **20,** 491–518.

McDermott, G., Prince, S. M., Freer, A. A., Hawthornthwaite-Lawlee, A. M., Papiz, M. Z., Cogdell, R. J., and Isaacs, N. W. (1995) Crystal structure of an integral membrane light-harvesting complex from photosynthetic bacteria, *Nature* **374,** 517–525.

McGough, A., Way, M., and DeRosier, D. (1994) Determination of the alpha-actinin-binding site on actin-filaments by cryoelectron microscopy and image-analysis, *J. Cell Biol.* **126,** 433–443.

McEwen, B. F., Downing, K. H., and Glaeser, R. M. (1995) The relevance of dose-fractionation in tomography of radiation-sensitive specimens, *Ultramicroscopy* **60,** 357–373.

Miller, K. R. (1982) Three-dimensional structure of a photosynthetic membrane, *Nature* **300,** 53–55.

Mitra, A. K., van Hoek, A. N., Wiener, M. C., Verkman, A. S., and Yeager, M. (1995) The CHIP28 water channel visualized in ice by electron crystallography, *Nature Struct. Biol.* **2,** 726–729.

Mitsuoka, K., Hirai, T., Murata, K., Miyazawa, A., Kidera, A., Kimura, Y., and Fujiyoshi, Y. (1998) Charge distribution in the refined structure of bacteriorhodopsin based on electron crystallography, submitted.

Moffat, K., and Henderson, R. (1995) Freeze trapping of reaction intermediates, *Curr. Opin. Struct. Biol.* **5,** 656–663.

Montoya, G., Cyrklaff, M., and Sinning, I. (1995) Two-dimensional crystallization and preliminary structure analysis of light harvesting II (B800–850) complex from the purple bacterium *Rhodovulum sulfidophilum*, *J. Mol. Biol.* **250,** 1–10.

Morris, E. P., Hankamer, B., Zheleva, D., Friso, G., and Barber, J. (1997) The three-dimensional structure of a photosystem II core complex determined by electron crystallography, *Structure* **5,** 837–849.

Nakasako, M., Kataoka, M., Amemiya, Y., and Tokunaga, F. (1991) Crystallographic characterization by X-ray diffraction of the M-intermediate from the photo-cycle of bacteriorhodopsin at room temperature, *FEBS Lett.* **292,** 73–75.

Nakazato, K., Toyoshima, C., Enami, I., and Inoue, Y. (1996) Two-dimensional crystallization and cryo-electron microscopy of photosystem II, *J. Mol. Biol.* **257,** 225–232.

Nogales, E., Wolf, S. G., Zhang, S. X., and Downing, K. H. (1995) Preservation of 2-D crystals of tubulin for electron crystallography, *J. Struct. Biol.* **115,** 199–208.

Nogales, E., Wolf, S. G., and Downing, K. H. (1998) Structure of the αβ tubulin dimer, by electron crystallography, *Nature* **391,** 199–203.

Oesterhelt, D., Tittor, J., and Bamberg, E. (1992) A unifying concept for ion translocation by retinal proteins, *J. Bioenerg. Biomem.* **24,** 181–191.

Ovchinnikov, Y. A., Abdulaev, N. G., Feigina, M. Y., Kiselev, A. V., and Lobanov, N. A. (1979) The structural basis of the functioning of bacteriorhodopsin: an overview, *FEBS Lett.* **100,** 219–224.

Pebay-Peyroula, E., Rummel, G., Rosenbusch, J. P., and Landau, E. M. (1997) X-ray structure of bacteriorhodopsin at 2.5 Å from microcrystals grown in lipidic cubic phases, *Science* **277,** 1676–1681.

Perkins, G., Goodenough, D., and Sosinsky, G. (1997) Three-dimensional structure of the gap junction connexon, *Biophys. J.* **72,** 533–544.

Porter, K. (1986) High-voltage electron-microscopy, *J. Electr. Micr. Techn.* **4,** 142–145.

Preston, G. M., Carroll, T. P., Guggino, W. B., and Agre, P. (1992) Appearance of water channels in *Xenopus* oocytes expressing red cell CHIP28 protein, *Science* **256,** 385–387.

Rachel, R., Engel, A. M., Huber, R., Stetter, K.-O., and Baumeister, W. (1990) A porin-type protein is the main constituent of the cell envelope of the ancestral eubacterium *Thermotoga maritima*, *FEBS Lett.* **262,** 64–68.

Rayment, I., Holden, H. M., Whittaker, M., Yohn, C. B., Lorenz, M., Holmes, K. C., and Milligan, R. A. (1993) Structure of the actin-myosin complex and its implications for muscle contraction, *Science* **261,** 58–65.

Renken, C., Perkins, G., Martone, M., Edelman, V., Deerinck, T., Ellisman, M., and Frey, T. (1997) Three-dimensional reconstructions of mitochondria by electron tomography, *Micr. Res. Techn.* **36,** 349–350.

Revel, J.-P., and Karnovsky, J. J. (1967) Hexagonal array of subunits in intercellular junctions of the mouse heart and liver, *J. Cell Biol.* **33,** C7-C12.

Rhee, K.-H., Morris, E. P., Zheleva, D., Hankamer, B., Kühlbrandt, W., and Barber, J. (1997) Two-dimensional structure of plant photosystem II at 8Å resolution, *Nature* **389,** 522–526.

Robertson, J. D. (1963) The occurence of a subunit pattern in the unit membrane of club ending in Mauthner cell synapses in goldfish brains, *J. Cell Biol.* **19,** 201–221.

Rossman, M. G., Olson, N. H., Kolatkar, P. R., Oliveira, M. A., Cheng, R. H., Greve, J. M., McClelland, A., and Baker, T. S. (1994) Crystallographic and cryo EM analysis of virion-receptor interactions, *Arch. Virol.* **S9,** 531–541.

Rothschild, K. J. (1992) FTIR difference spectroscopy of bacteriorhodopsin: toward a molecular model, *J. Bioenerg. Biomem.* **24,** 147–167.

Santini, C., Tidu, V., Tognon, G., Ghiretti Magaldi, A., and Bassi, R. (1994) Three-dimensional structure of higher plant photosystem II reaction centre and evidence for its dimeric organization, *Eur. J. Biochem.* **221,** 307–315.

Sass, H. J., Büldt, G., Beckmann, E., Zemlin, F., van Heel, M., Zeitler, E., Rosenbusch, J. P., Dorset, D. L., and Massalski, A. (1989) Densely packed β-structure at the protein-lipid interface of porin is revealed by high-resolution cryo-electron microscopy, *J. Mol. Biol.* **209,** 171–175.

Savage, H., Cyrklaff, M., Montoya, G., Kühlbrandt, W., and Sinning, I. (1996) Two-dimensional structure of light harvesting complex II (LHII) from the purple bacterium *Rhodovulum sulfidophilum* and comparison with LHII from *Rhodopseudomonas acidophila*, *Structure* **4,** 243–252.

Scarborough, G. A. (1994) Large single-crystals of the *Neurospora crassa* plasma-membrane H^+-ATPase - an approach to the crystallization of integral membrane proteins, *Acta Crystallogr.* **D50,** 643–649.

Schertler, G. F. X., Villa, C., and Henderson, R. (1993) Projection structure of rhodopsin, *Nature* **362,** 770–772.

Schertler, G. F. X., and Hargrave, P. A. (1995) Projection structure of frog rhodopsin in two crystal forms, *Proc. Natl. Acad. Sci. USA* **92,** 11578–11582.

Schirmer, T., and Rosenbusch, J. P. (1991) Prokaryotic and eukaryotic porins, *Curr. Opin. Struct. Biol.* **1,** 539–545.

Schirmer, T., Keller, T. A., Wang, Y.-F., and Rosenbusch, J. P. (1995) Structural basis for sugar translocation through maltoporin channels at 3.1 Å resolution, *Science* **267,** 512–514.

Schmid, M. F., Agris, J. M., Jakana, J., Matsudaira, P., and Chiu, W. (1994) 3-dimensional structure of a single filament in the limulus acrosomal bundle - scruin binds to homologous helix-loop-beta motifs in actin, *J. Cell Biol.* **124,** 341–350.

Schmidt-Krey, I., Murata, K., Hirai, T., Morgenstern, R., Fujiyoshi, Y., and Hebert, H. (1998) The projection structure of the membrane protein microsomal glutathione transferase at 3 Å resolution as determined from two-dimensional crystals of the p2 form, in preparation.

Schmitz, H., Reedy, M. C., Reedy, M. K., Tregear, R. T., Winkler, H., and Taylor, K. A. (1996) Electron tomography of insect flight muscle in rigor and AMPPNP at 23°C, *J. Mol. Biol.* **264,** 279–301.

Schmutz, M., and Brisson, A. (1996) Analysis of carbon film planarity by reflection light microscopy, *Ultramicroscopy* **63,** 263–272.

Schobert, B., and Lanyi, J. K. (1982) Halorhodopsin is a light-driven chloride pump, *J. Biol. Chem.* **257,** 10306–10313.

Shi, D., Hsiung, H.-H., Pace, R. C., and Stokes, D. L. (1995) Preparation and analysis of large, flat crystals of Ca^{2+}-ATPase for electron crystallography, *Biophys. J.* **68,** 1152–1162.

Sikerwar, S. S., Downing, K. H., and Glaeser, R. M. (1991) 3-dimensional structure of an invertebrate intercellular communicating junction, *J. Struct. Biol.* **106,** 255–263.

Simón, M., Mathes, A., Blanch, A., and Engelhardt, H. (1996) Characterization of a porin from the outer membrane of *Vibrio anguillarum*, *J. Bacteriol.* **178,** 4182–4188.

Smith, T. J., Chase, E. S., Schmidt, T. J., Olson, N. H., and Baker, T. S. (1996) Neutralizing antibody to human rhinovirus-14 penetrates the receptor-binding canyon, *Nature* **383,** 350–354.

Soderberg, B.-O., Sjoberg, B.-M., Sonnerstam, U., and Branden, C.-I. (1978) Three-dimensional structure of thioredoxin induced by bacteriophage T4, *Proc. Natl. Acad. Sci. USA* **75,** 5827–5830.

Stahlberg, H., Dubochet, J., Vogel, H., and Ghosh, R. (1998) Are light-harvesting I complexes from *Rhodospirillum rubrum* arranged around the reaction centre in a square geometry?, submitted.

Stark, W., Kühlbrandt, W., Wildhaber, H., Wehrli, E., and Mühlethaler, K. (1984) The structure of the photoreceptor unit of *Rhodopseudomonas viridis*, *EMBO J.* **3,** 777–783.

Stokes, D. L. (1997) Keeping calcium in its place: Ca^{2+}-ATPase and phospholamban, *Curr. Opin. Struct. Biol.* **7,** 550–556.

Subramaniam, S., Gerstein, M., Oesterhelt, D., and Henderson, R. (1993) Electron diffraction analysis of structural changes in the photocycle of bacteriorhodopsin, *EMBO J.* **12,** 1–8.

Subramaniam, S., Faruqi, A. R., Oesterhelt, D., and Henderson, R. (1997) Electron diffraction studies of light-induced conformational changes in the Leu-93 → Ala bacteriorhodopsin mutant, *Proc. Natl. Acad. Sci. USA* **94,** 1767–1772.

Taylor, K. A., and Glaeser, R. M. (1974) Electron diffraction of frozen, hydrated protein crystals, *Science* **186,** 1036–1037.

Taylor, K. A., and Varga, S. (1994) Similarity of three-dimensional micro-crystals of detergent-solubilized (Na^+/K^+)-ATPase from pig kidney and Ca^{2+}-ATPase from skeletal muscle sarcoplasmic reticulum, *J. Biol. Chem.* **269,** 10107–10111.

Trus, B. L., Roden, R. B. S., Greenstone, H. L., Vrhel, M., Schiller, J. T., and Booy, F. P. (1997) Novel structural features of bovine papillomavirus capsid revealed by a three-dimensional reconstruction to 9 Å resolution, *Nature Struct. Biol.* **4,** 413–420.

Tsiotis, G., Walz, T., Spyridaki, A., Lustig, A., Engel, A., and Ghanotakis, D. (1996) Tubular crystals of a photosystem II core complex, *J. Mol. Biol.* **259,** 241–248.

Unger, V. M., and Schertler, G. F. X. (1995) Low resolution structure of bovine rhodopsin determined by electron cryomicroscopy, *Biophys. J.* **68,** 1776–1786.

Unger, V. M., Kumar, N. M., Gilula, N. B., and Yeager, M. (1997a) Projection structure of a gap junction membrane channel at 7 Å resolution, *Nature Struct. Biol.* **4,** 39–43.

Unger, V. M., Hargrave, P. A., Baldwin, J. M., and Schertler, G. F. X. (1997b) Arrangement of rhodopsin transmembrane α-helices, *Nature* **389,** 203–206.

Unwin, P. N. T., and Henderson, R. (1975) Molecular structure determination by electron microscopy of unstained crystalline specimens, *J. Mol. Biol.* **94,** 425–440.

Unwin, P. N. T., and Zampighi, G. (1980) Structure of the junction between communicating cells, *Nature* **283,** 545–549.

Unwin, P. N. T. (1983) Calcium-mediated changes in gap junction structure: evidence from the low angle X-ray pattern, *J. Cell. Biol.* **97,** 1459–1466.

Unwin, P. N. T., and Ennis, P. D. (1984) Two configurations of a channel-forming membrane protein, *Nature* **307,** 609–613.

Unwin, N. (1986) Is there a common design for cell membrane channels?, *Nature* **323,** 12–13.

Valpuesta, J. M., Carrascosa, J. L., and Henderson, R. (1994) Analysis of electron microscope images and electron diffraction patterns of thin crystals of ϕ29 connector in ice, *J. Mol. Biol.* **240,** 281–287.

Vonck, J. (1996) A three-dimensional difference map of the N intermediate in the bacteriorhodopsin photocycle: part of the F helix tilts in the M to N transition, *Biochemistry* **35,** 5870–5878.

Walz, T., Typke, D., Smith, B. L., Agre, P., and Engel, A. (1995) Projection map of aquaporin-1 determined by electron crystallography, *Nature Struct. Biol.* **2,** 730–732.

Walz, T., and Ghosh, R. (1997a) Two-dimensional crystallization of the light-harvesting I- reaction centre photounit from *Rhodospirillum rubrum*, *J. Mol. Biol.* **265,** 107–111.

Walz, T., Hirai, T., Murata, K., Heymann, J. B., Mitsuoka, K., Fujiyoshi, Y., Smith, B. L., Agre, P., and Engel, A. (1997b) The three-dimensional structure of aquaporin-1, *Nature* **387,** 624–627.

Walz, T., Jamieson, S. J., Bowers, C. M., Bullough, P. A., and Hunter, C. N. (1998) Projection structures of three photosynthetic complexes from Rhodobacter sphaeroides: LH2 at 6Å, LH1 and RC-LH1 at 25 Å, in preparation.

Wang, D. N., and Kühlbrandt, W. (1991) High-resolution electron crystallography of light-harvesting chlorophyll *a*/*b*-protein complex in three different media, *J. Mol. Biol.* **217,** 691–699.

Weiss, M. S., Wacker, T., Weckesser, J., Welte, W., and Schulz, G. E. (1990) The three-dimensional structure of porin from *Rhodobacter capsulatus* at 3 Å resolution, *FEBS Lett.* **267,** 268–272.

Weiss, M. S., and Schulz, G. E. (1992) Structure of porin refined at 1.8 Å resolution, *J. Mol. Biol.* **227,** 493–509.

Wilce, M. C. J., and Parker, M. W. (1994) Structure and function of glutathione *S*-transferases, *Biochim. Biophys. Acta* **1205,** 1–18.

Williams, R. C., and Fisher, H. W. (1970) Electron microscopy of tobacco mosaic virus under conditions of minimal beam exposure, *J. Mol. Biol.* **52,** 121–123.

Zhuang, J., Engel, A., Pagès, J.-M., and Bolla, J.-M. (1997) The *Campylobacter jejuni* porin trimers pack into different lattice types when reconstituted in the presence of lipid, *Eur. J. Biochem.* **244,** 575–579.